

An Open-Loop Approach to Study the Stochastic Properties

Inauguraldissertation
zur
Erlangung der Würde eines Doktors der Philosophie
vorgelegt der
Philosophisch-Naturwissenschaftlichen Fakultät
der Universität Basel

von

Farzaneh Maleki
aus Malayer, Iran

Basel, 2016

Originaldokument gespeichert auf dem Dokumentenserver der Universität Basel
edoc.unibas.ch



This work is licenced under the agreement
Attribution Non-Commercial No Derivatives - 3.0 Switzerland (CC BY-NC-ND 3.0 CH).

The complete text may be reviewed here:
creativecommons.org/licenses/by-nc-nd/3.0/ch/deed.en

Genehmigt von der Philosophisch-Naturwissenschaftlichen Fakultät
auf Antrag von

Prof. Attila Becskei und Prof. Helmut Harbrecht

Basel, den 21. Juni 2016

Prof. Dr. Jörg Schibler

Dekan



Namensnennung-Keine kommerzielle Nutzung-Keine Bearbeitung 3.0
Schweiz
(CC BY-NC-ND 3.0 CH)

Sie dürfen: **Teilen** - den Inhalt kopieren, verbreiten und zugänglich machen

Unter den folgenden Bedingungen:



Namensnennung – Sie müssen den Namen des Autors/Rechteinhabers in der von ihm festgelegten Weise nennen.



Keine kommerzielle Nutzung – Sie dürfen diesen Inhalt nicht für kommerzielle Zwecke nutzen.



Keine Bearbeitung erlaubt – Sie dürfen diesen Inhalt nicht bearbeiten, abwandeln oder in anderer Weise verändern.

Wobei gilt:

- **Verzichtserklärung** – Jede der vorgenannten Bedingungen kann **aufgehoben** werden, sofern Sie die ausdrückliche Einwilligung des Rechteinhabers dazu erhalten.
- **Public Domain (gemeinfreie oder nicht-schützbarer Inhalte)** – Soweit das Werk, der Inhalt oder irgendein Teil davon zur Public Domain der jeweiligen Rechtsordnung gehört, wird dieser Status von der Lizenz in keiner Weise berührt.
- **Sonstige Rechte** – Die Lizenz hat keinerlei Einfluss auf die folgenden Rechte:
 - Die Rechte, die jedermann wegen der Schranken des Urheberrechts oder aufgrund gesetzlicher Erlaubnisse zustehen (in einigen Ländern als grundsätzliche Doktrin des **fair use** bekannt);
 - Die **Persönlichkeitsrechte** des Urhebers;
 - Rechte anderer Personen, entweder am Lizenzgegenstand selber oder bezüglich seiner Verwendung, zum Beispiel für **Werbung** oder Privatsphärenschutz.
- **Hinweis** – Bei jeder Nutzung oder Verbreitung müssen Sie anderen alle Lizenzbedingungen mitteilen, die für diesen Inhalt gelten. Am einfachsten ist es, an entsprechender Stelle einen Link auf diese Seite einzubinden.

Quelle: <http://creativecommons.org/licenses/by-nc-nd/3.0/ch/> Datum: 12.11.2013

To the love of my life

Amir

Abstract

Randomness is an inevitable aspect of biological networks. It has been long accepted that variability of components in a network can propagate throughout the network. In this thesis, we introduce a method that allows us to decompose the total variability of a single component into individual contributions from the other components in a network. Our method of noise decomposition helps us investigate key parameters and their relative impact on the total normalized noise and also allows us to illustrate the importance of different system modifications by adding or omitting biological processes. With our generally applicable noise decomposition method, we are able to determine the strength of individual correlations induced by different co-regulation processes that connect different components of a network. In bistable systems, variability can occur through stochastic transitions from one steady state to another. Noise induced transitions between two steady states are difficult to calculate due to the intricate interplay between nonlinear dynamics and noise in bistable positive feedback loops. We open multicomponent feedback loops at the slowest variables in order to calculate the transition rates from one steady state to another. By reclosing the feedback loop, we calculate the mean first passage time (MFPT) using the Fokker-Planck equation. It is important to emphasize that the accurate approximation of the open-loop results is not a sufficient condition for a good prediction of the MFPT. We show that only the opening at the slowest variable warrants an accurate prediction of MFPT. Multiplicative interactions among different components can introduce correlations among noises. We show that the introduced correlations affect the mean and variance of the open-loop function and consequently increase the transition rate between two steady states in the closed-loop system. Our results indicate that the open-loop approach can contribute to the theoretical prediction of the MFPT. The theoretical results are shown to be in good agreement with the results of stochastic simulation.

Contents

Contents	v
1 Introduction	1
1.1 Dynamical system	1
1.1.1 Bifurcations	2
1.1.2 Bistability	3
1.2 Stochastic Processes	3
1.2.1 Master equation	5
1.2.2 Stochastic differential equation	5
1.2.3 Fokker-Planck Equations	7
1.3 Mean first passage time	8
1.4 Stochastic simulation algorithm	10
2 Results	11
2.1 Noise decomposition	14
2.1.1 Example - Translational regulation	16
2.1.2 Example - Transcriptional regulation	17
2.1.3 Example - RNA enzymatic decay	18
2.2 Co-regulation processes	19
2.2.1 Example - Co-regulation processes	20
2.3 Mean first passage time (MFPT)	21
2.3.1 Example - Feedback loop system with a single component	22
2.4 Characterization of drift by the open-loop approach	24
2.5 Calculation of diffusion with uncorrelated white noises	25
2.5.1 Example - Positive feedback loop system comprising RNA and protein	27
2.5.2 Example - Opening the loop at the slowest components is necessary in MFPT calculation	30
2.6 Hidden nonlinearities	35
2.7 Calculation of diffusion with correlated white noises	35

2.7.1	Example - The effect of multiplicative interactions on MFPT	38
2.7.2	Example - The effect of different nonlinearities on MFPT	44
2.8	Experimental applications of the open-loop approach	45
2.8.1	Example - A two-component system consisting of an enzyme and a protein	46
2.8.2	Example - A four-component system consisting of two RNAs and two proteins	47
2.8.3	Example - The effect of homodimerization and cooperativity on transition rate	48
3	Conclusions	57
	Bibliography	64

Chapter 1

Introduction

Systems biology, as an inter-disciplinary field of science, investigates biological species, molecular interactions, and how these interactions give rise to specific behaviors in biological systems. Mathematical modeling has been long recognized as a powerful tool to analyze complex interactions between components of biological networks by proposing testable hypotheses and designing computational and theoretical models that can be validated by the experimental data. Mathematical models are usually represented by dynamical systems since the state of living systems evolve through the time. The main idea behind using dynamical systems is to mathematically represent different cellular states as attractors of the system which in turn define different cellular decisions. The emergence of such attractors are dependent on the structure of biological networks. In particular, the existence of positive feedback loops in gene regulatory networks is a necessary condition for the network to have multiple attractors, a phenomenon known as multistability.

1.1 Dynamical system

Dynamical systems are mathematical formulations of physical or biological processes by a family of evolution operators φ^t , parametrized by time t , that function in state space X (Figure 1.1). Dynamical systems can model deterministic events where there is a unique state for each time point, or model stochastic processes where there is a distribution of possible states for a time point [15]. The time evolution of many systems in nature can be predicted using their corresponding dynamical systems. The dimension of state space determines the dimension of the dynamical system. The state of a system at any individual time point is determined by its corresponding time evolution operator provided that the initial state x_0 is given. Parameter dependent dynamical systems can

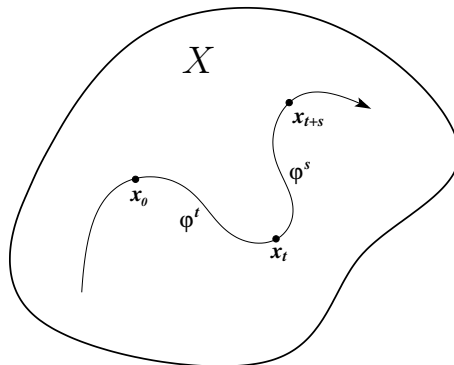


Figure 1.1: Evolution operator.

be represented by a set of first order ordinary differential equations (ODEs)

$$\dot{x}(t) = \frac{dx(t)}{dt} = f(x(t), \mu), \quad \mu, x \in \mathbb{R}^n, \quad (1.1)$$

with the unique time evolution operator φ^t

$$x(t) = \varphi^t(x_0, \mu), \quad x_0 = x(0),$$

that satisfies equation (1.1). Steady states of dynamical system (1.1) are given by $x_s \in X$ such that $f(x_s; \mu) = 0$. Steady states can be either stable and absorb all nearby trajectories or unstable and repel them.

1.1.1 Bifurcations

The quantity and stability of steady states of a dynamical system may change as the parameter values are varied. When this change, which is also called qualitative change, happens, a bifurcation is said to emerge in the state space of a given dynamical system [55]. The qualitative change can occur generically by changing the value of one (co-dimension one) or more (co-dimension n) parameters. Bifurcations can be classified into local bifurcations analyzed by local stability analysis of steady states, and global bifurcations, which occur as a result of collision of invariant sets of a system. Fold bifurcation (saddle-node bifurcation) is an example of local co-dimension one bifurcations [26] in which two steady states collide and annihilate each other at a specific parameter value which is called the bifurcation point in the parameter space (Figure 1.2). Suppose that the dynamical system (1.1) with a smooth f , has a steady state x_c at $\mu = \mu_c$ that satisfies

$$f(x_c, \mu_c) = 0, \quad \frac{d}{dx}f(x_c, \mu_c) = 0. \quad (1.2)$$

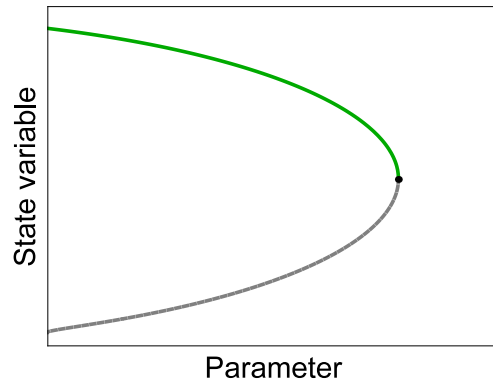


Figure 1.2: The fold bifurcation diagram. On the left half of the plane, system (1.2) has two branches of steady states, one being stable and the other unstable. Moving from left to right, the two branches of steady states collide and disappear at the bifurcation point.

System (1.2) undergoes a generic fold bifurcation at steady state x_c if

$$\frac{d^2}{dx^2}f(x_c, \mu_c) \neq 0, \quad \frac{d}{d\mu}f(x_c, \mu_c) \neq 0.$$

The above inequalities are called the non-degeneracy and the transversality conditions, respectively.

1.1.2 Bistability

In a dynamical system, bistability means that the system has two stable steady states and, depending on the initial conditions, the system tends to one of the two steady states. In the potential landscape, a bistable system has two wells separated by a peak which is the unstable steady state. Bistability, which can be generated by a positive feedback loop with ultrasensitivity, is a key element to study the cellular memory in biological networks. One characteristic of bistable systems is that they demonstrate a hysteresis behavior. The hysteresis curve indicates the range of parameter values for which a system has two stable steady states (Figure 1.3).

1.2 Stochastic Processes

A stochastic process is a random evolution of a set of variables over the course of time. Random variables (state or/and time) can be discrete or/and continuous [30]. More accurately, a stochastic process is a collection of random variables X on probability space Ω indexed by time t , $\{X_t, t \in T\}$. The future state of

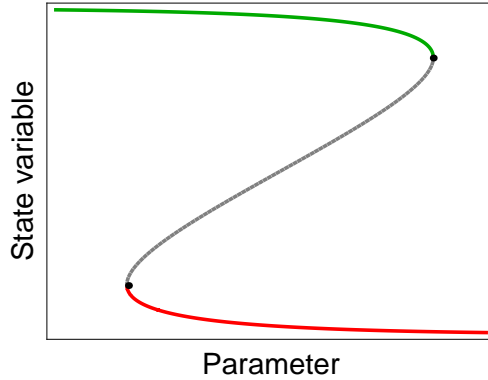


Figure 1.3: Hysteresis curve. The fold bifurcation points are determined by the two knees of the curve (black disk). For the values of a parameter between the two knees, system has one unstable (dashed gray) and two stable steady states (solid red and green).

a stochastic process X_t can be determined by its past and present states. A Markovian process (Figure 1.4), known as a memoryless process, is a stochastic process X_t in which the future of the process depends only on its present state. This means that X_{t_k} depends only on $X_{t_{k-1}}$

$$P(X_{t_k}|X_{t_1}, \dots, X_{t_{k-1}}) = P(X_{t_k}|X_{t_{k-1}}).$$

The above definition (known as Markov property) combined with conditional probability allows us to reconstruct the hierarchy

$$P(X_1, X_2, X_3|X_1, X_2) = P(X_3|X_2)P(X_2|X_1)P(X_1).$$

The joint probability distribution function is then obtained easily by integrating the above equation to get

$$P(X_3|X_1) = \int_{-\infty}^{\infty} P(X_3|X_2)P(X_2|X_1)dX_2,$$

which is known as the Chapman-Kolmogorov equation [30]. A Markovian process can be described through Chapman-Kolmogorov equation as long as the process has a finite and independent mean and variance. The continuous stochastic processes along with the Markov property are known as Wiener processes. A Wiener process $W(t)$ is a continuous stochastic process characterized by normal distribution $\mathcal{N}(0, \sigma t)$ which means that the fluctuation arises linearly in time. The Wiener processes with irregular motions are key processes to describe complicated stochastic processes. The standard Wiener process has the

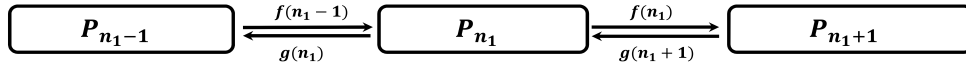


Figure 1.4: Markovian process is a stochastic process in which the future of the process depends only on its present state.

zero initial condition $W(0) = 0$. The time evolution of a Wiener process can be represented by a Gaussian white noise $\xi(t)$

$$\frac{d}{dt}W(t) = \xi(t).$$

1.2.1 Master equation

The Chapman-Kolmogorov equation corresponds to the probability of being at point x at time $t + dt$ given the initial position at time t

$$P(x|y, t + dt) = \int_{-\infty}^{\infty} P(x|z, t)P(z|y, dt)dz.$$

The transition probability from x to y for a short time period dt can be expressed by adding the probability of transition from x to y to the probability of having no transition during the time dt . This implies

$$P(y|x, dt) = \left(1 - dt \int_{-\infty}^{\infty} w(y|x)dy\right)\delta(y - x) + dtw(y|x) + o(dt),$$

where $\delta(y - x) = P(y|x, 0)$ and $w(y|x)$ is the transition probability from x to y in a small time increment dt . By re-arranging Chapman-Kolmogorov equation and dividing the result by dt , one gets

$$\frac{d}{dt}P(x|x_0, t) = \int_{-\infty}^{\infty} [w(x|y)P(y|x_0, dt) - w(y|x)P(x|x_0, dt)] dy,$$

which describes the time evolution of the probability of a system with regard to a continuous time variable t , and is known as master equation [53].

1.2.2 Stochastic differential equation

By repeating a stochastic process many times, we will observe some repeated averaged behaviors which are roughly in agreement by the deterministic description plus some fluctuations. This indicates the separation of the deterministic part (\bar{X}) of a stochastic variable X from the fluctuation α , which is proportional

to the square root of the system volume

$$\frac{N}{\Omega} = X = \bar{X} + \frac{\alpha}{\sqrt{\Omega}}, \quad (1.3)$$

where N and X represent the number of molecules and the concentration, respectively. In a network, each fluctuating component is presented in the form of equation (1.3). The time evolution of a stochastic variable X in form of equation (1.3) leads to the definition of the stochastic differential equation (SDE)

$$\frac{d}{dt}X = F(\bar{X}) + \sigma_1 g_1(X) \xi(t) + \sigma_2 g_2(X) \zeta(t), \quad (1.4)$$

where $F(\bar{X})$ represents the deterministic part of the system and $\xi(t)$ and $\zeta(t)$ can represent intrinsic and extrinsic fluctuations with the intensity $\sigma_i = \frac{1}{\sqrt{\Omega}}$. The fluctuations can be additively [28] or multiplicatively [10] incorporated into a system. From equation (1.4), the total diffusion is given by

$$D_{total} = \underbrace{\sigma_1^2 g_1^2(X)}_{D_{Intrinsic}} + \underbrace{\sigma_2^2 g_2^2(X)}_{D_{Extrinsic}}. \quad (1.5)$$

It should be noted that in real systems, fluctuations have non-zero auto-correlation time. White noise is an idealized replacement of a time-dependent noise with considerably short correlation time. This short memory will result in a dependency between the state variable and the fluctuations, and can change the expectation value of $X(t)$. Such dependency represents a correlation between the system and the environmental noise known as extrinsic fluctuation [16]. From the mathematical point of view, the absence or presence of such correlation can be imposed to the system by different integration methods. In the absence of correlation between the dynamic of the system and the stochasticity, the drift can be obtained based on Riemann integration and the method is known as Ito

$$H(\bar{X}) = F(\bar{X}), \quad (1.6)$$

while in the presence of the mentioned correlation, Lebesgue integration will be used and the method is known as Stratonovich

$$H(\bar{X}) = F(\bar{X}) + \frac{1}{4} \frac{d}{dX} D_{Extrinsic}. \quad (1.7)$$

Although both methods are defined based on Brownian motion and describe the same quantity, the results are different. In a given system, different sources of stochasticity might have a common origin and be cross-correlated [6, 7]. A

white cross-correlation between $\xi(t)$ and $\zeta(t)$ in equation (1.4) will modify the term of diffusion (1.5) as follows

$$D_{total} = \underbrace{\sigma_1^2 g_1^2(X)}_{D_{Intrinsic}} + \underbrace{\sigma_2^2 g_2^2(X) + 2\rho \sigma_1 \sigma_2 g_1(X) g_2(X)}_{D_{Extrinsic}}, \quad (1.8)$$

in which $\rho = \frac{\langle \xi(t), \zeta(t') \rangle}{\sigma_1 \sigma_2}$ represents the correlation between $\xi(t)$ and $\zeta(t)$.

1.2.3 Fokker-Planck Equations

In multidimensional systems with strong nonlinearities, master equations are too complicated and difficult to solve. A large effort has been made to design methods to simplify or approximate the master equation analytically or numerically [19, 20, 27, 42]. The Fokker-Planck equation (FPE) as an approximation of the master equation is an alternative approach for systems with complexities [44]. FPE is the second-order truncation of Kramers-Moyal expansion of the master equation [35, 40] with respect to system size Ω

$$\frac{d}{dt}P(X) = -\frac{\partial}{\partial X}H(X)P(X) + \frac{1}{2\Omega} \frac{\partial^2}{\partial X^2}D_{total}(X)P(X), \quad (1.9)$$

where $H(X)$ and $D_{total}(X)$ are the drift and diffusion, respectively. In biology, the system size is the cell volume. The Fokker-Planck equation describes the dynamics of probability distribution functions over time by using partial differential equations. Equation (1.9) can be nonlinear with respect to the stochastic variable X even though it is linear with respect to probability distribution $P(X)$. Equations (1.4) and (1.9) can be taken identical if the corresponding histogram of a large collection of different stochastic trajectories satisfying equation (1.4) satisfies equation (1.9). Hence, the dynamics of the probability distribution of a stochastic process modeled by (1.4) can be represented by (1.9) in which the tails of the probability distribution describe the size of variability. It should be noted that (1.9) is obtained by the assumption of small perturbation, and hence the larger fluctuations are, the less accurate the approximation will be [54]. The first term in equation (1.9) contains no fluctuation and can be interpreted as the deterministic part of the system. The second term in equation (1.9) corresponds to the second order of Kramers-Moyal expansion of the master equation and describes the lowest order of fluctuations. The time evolution of the expectation value \bar{X} and covariance matrix C corresponding to (1.9) can be

linearized around the expectation value

$$\begin{aligned}\dot{\bar{X}} &= H(\bar{X}) = F(\bar{X}) + \frac{1}{2} \sum_{i,j} \frac{d^2 F(\bar{X})}{dX_i dX_j} C_{ij}, \\ \dot{C} &= JC + (JC)^T + B,\end{aligned}\tag{1.10}$$

where $J = \frac{d}{d\bar{X}} F(\bar{X})$ represents the Jacobian matrix. Matrix B contains the intrinsic diffusion of all components and is given by

$$B = S \text{Diag}(V) S^T,$$

where S and V are the stoichiometry matrix and the reaction rate vector, respectively. The drift $H(\bar{X})$ in the first equation in (1.10) is equivalent to equations (1.6) and (1.7). In the presence of multiple extrinsic fluctuations, the drift is represented by Stratonovich interpretation. Linearization of equation (1.10) with respect to \bar{X} is known as linear noise approximation (LNA) and can be used for the multidimensional networks which are not strongly nonlinear [9]. Equations (1.10) are obtained based on local perturbation which means that the results are valid at the vicinity of the corresponding basin of attraction. This criterion describes the physical meaning of local and global stability and shows the fact that such approximation cannot be used for global properties like mean first passage time (MFPT). Normalization of the variance with mean squared of component i results in the coefficient of variation

$$CV_i^2 = \eta_i^2 = \frac{C_{ii}^2}{\bar{X}_{ii}^2}.\tag{1.11}$$

The coefficient of variation, known also as normalized noise, is applicable to positive statistical samples like biological data.

1.3 Mean first passage time

In a multistable system, a trajectory can not deterministically cross the boundary of a basin of attraction while in a stochastic system, due to fluctuations, trajectories may reach the boundary in a finite time [32]. One should distinguish between the exit time ($T = \infty$) predicted from a deterministic system and the switching time ($T < \infty$) obtained from the stochastic system. The first passage problem is referred to the time it takes the state of a system to reach a point (or a boundary) for the first time which is denoted by $\tau(X)$ and associated with a probability density $f_\tau(X, t)$. Suppose that the probability distribution has an

absorbing boundary R and a reflecting boundary R^* at which

$$P(R) = 0, \quad \frac{d}{dX}P(X)|_{X=R^*} = 0 \quad (1.12)$$

The probability density $f_\tau(X, t)$ can be interpreted as the time evolution of the survival probability $S(X, t)$ which is the probability being remained at X at time t

$$f_\tau(X, t) = -\frac{d}{dt}S(X, t) = -\frac{d}{dt} \int_{-\infty}^R P(X|X_0)dX. \quad (1.13)$$

Mean first passage time $T(X)$, the average time for a random variable to switch from one state to another, is therefore

$$T(X) = \int_0^\infty t f_\tau(X, t) dt. \quad (1.14)$$

From equations (1.9), (1.13) and (1.14), one can obtain

$$H(X) \frac{d}{dX}T(X) + \frac{1}{2\Omega} D_{total}(X) \frac{\partial^2}{\partial X^2}T(X) = -1 \quad (1.15)$$

with the boundary conditions

$$T(R) = 0, \quad \frac{d}{dX}T(X)|_{X=R^*} = 0. \quad (1.16)$$

Therefore, mean first passage time from X_l to X_h is obtained by solving equation (1.15) with the boundary condition (1.16)

$$T(X_l \rightarrow X_h) = \int_{X_l}^{X_h} \frac{1}{V(Y)} \left(\int_0^Y \frac{V(X)}{D_{total}(X)} dX \right) dY, \quad (1.17)$$

where

$$V(X) = - \int \frac{H(X)}{D_{total}(X)} dX,$$

is the effective potential function. Kramers escape rate [2, 3] as an approximation of (1.17) describes the MFPT between local minimum X_s and maximum X_u in a potential landscape

$$T(X_s) - T(X_u) = \frac{2\pi}{\sqrt{|V''(X_s) V''(X_u)|}} e^{|V(X_s) - V(X_u)|}, \quad (1.18)$$

where $V''(X)$ is the second derivative of the effective potential function with respect to the state variable X .

1.4 Stochastic simulation algorithm

A common approach to investigate stochasticity is the stochastic simulation algorithm (SSA). Each trajectory of a single SSA represents an exact sample of the probability distribution function that is the solution of the master equation. The most well-known stochastic simulation algorithm has been introduced by Gillespie [13]. One assigns an initial number of components and repeats a loop until the system reaches the predefined termination conditions. The loop includes five steps as follows:

1. Initialize the number of molecules (X) in the system. Generate random numbers r_1 and r_2 .
2. Calculate the probabilities for production and degradation of each component for the next step based on the propensity vector $a_i(X)$.
3. Update the time τ of the occurrence of the next reaction

$$\tau = -\ln\left(\frac{r_1}{\sum a_i(X)}\right).$$

4. Determine the next reaction to occur. The next reaction R_j has the smallest integer j satisfying

$$\sum_{i=1}^j a_i(X) > r_2 a_0(X).$$

5. Update the number of components based on the chosen reaction.

Chapter 2

Results

Randomness is an inevitable feature of biological interactions. Biological components fluctuate due to the individual events considered as intrinsic noise or due to the fluctuations in the environment known as the extrinsic noise. In a network composed of different components, fluctuations in specific components count as intrinsic noise for the components themselves and a potential source of extrinsic noise for the other components [45, 47, 48]. For example, in transcriptional regulation processes, transitions among different states of promoters that control transcription [34, 43] or processes involved in degradation of RNAs like enzymatic degradation, can be defined as extrinsic sources of fluctuation to the level of RNAs. In order to characterize stochastic features of a system based on the noise effects, it is necessary to decompose the randomness in a network based on individual sources of noise. Variabilities in different components may be strongly co-dependent, so any changes in the corresponding total probability distribution will potentially affect the marginal distribution as well. This codependency shows the correlation between components and the environmental stochasticity and can be imposed to the system through the Stratonovich interpretation [16]. Existence of such correlation, which has a considerable effect on transition time between basins of attraction of the network [37], indicates that the drift is no longer static since it includes some stochasticity. In a multidimensional system which is under the effect of different sources of stochasticity, there are possibilities of coupling between different sources of noise. Components can directly or indirectly interact with each other which means that their stochastic effect will propagate through the system [36].

Coupling between components can introduce a hidden nonlinearity to the system due to the multiplication of the corresponding noises. Such multiplication can introduce a cross-correlation between fluctuation sources [6] which can happen

between the internal and environmental (external) fluctuations or two external noises. The strength of cross-correlation depends on different factors. Coupled components can amplify or attenuate stochastic effects and speed up network's response [41]. Time scale and the intensity of coupled fluctuations can change mean level and consequently the intrinsic noise [25]. The degree of stochasticity in a network depends on the structure and the parameters [4, 38]. Ignoring some fluctuations between different parts of a network may result in a wrong conclusion [22, 51, 52].

Stochasticity is a distinct feature of biological networks which can play a crucial role in the fate of the system. Kepler et al. [23] indicated that in systems under the effects of fluctuations, bimodality can be observed even if the deterministic system is monostable. Since in biological system the reactions are not necessarily first order, there is a possibility of cross-correlation between noises. Cross-correlation between noises in bistable systems has been introduced for the first time by Fulinski [11]. Later Mei et al. studied the steady state properties of a bistable system perturbed by cross-correlated noise with zero time correlation [33]. They showed that variations in the cross-correlation strength can cause a transition from unimodal to the bimodal distribution and therefore change the bimodal region in the parameter space. Experimental evidences indicate that the randomness has important consequences on a system behaviors like switching between different basins of attraction [10, 17]. It has been shown that the cross-correlation between perturbed production and decay rates can induce a switch process in gene transcriptional regulatory systems [29].

Mean first passage time (MFPT), the average time for a random variable to switch from one steady state to another, can be interpreted as the cellular memory which is a ubiquitous phenomenon in biology [8]. In physics, mean first passage time can be viewed as the transition time between local minima in a potential landscape. This can be considered as the time it takes for the components to escape from a potential well by crossing a potential barrier which is the unstable steady state. The escape rate approximation by crossing a potential barrier has been introduced for the first time by Kramers [24] in 1940. Chaudhuri et al. [7] studied the Kramers escape rate of a system under the influence of cross-correlated intrinsic and extrinsic noises. Recently Ghosh et al. [12] have used cross-correlated noises in order to show splitting of Kramers escape rate in symmetric triple wells.

A common method to approximate MFPT relies on the Fokker-Planck equation [40], which is typically used for one-dimensional systems. However, most biologically realistic feedback loops contain multiple components. Therefore, the fluctuation effects of all components of the system should be incorporated into the corresponding Fokker-Planck equation through the diffusion term. Although a major attempt has been made to investigate the effect of different sources of noise on what, no rigorous methods have been proposed to precisely identify the diffusion. In order to characterize the diffusion term based on different noise effects, it is necessary to decompose the randomness in a network based on individual sources of noise. The stochastic behavior in chemical kinetics can be interpreted through the master equation [53], which is well-known in analyzing stochastic properties. Unfortunately, the master equation can be analytically solved only for simple systems. A good alternative method to investigate random properties in complicated systems is the stochastic simulation algorithm. Since simulation of large networks with a large number of variables and parameters can be computationally expensive, an analytical approach might be more practical.

In this work, using Fokker-Planck equation (FPE) for multidimensional systems, we decompose the total normalized noise of specific components based on the contributions of different sources of fluctuation. An important feature of biological systems with coupled interactions is the presence of different co-regulation processes with different perturbation effects. It is interesting to investigate the strength of induced correlations due to an individual co-regulation process. Noise decomposition helps us decompose such correlations. It should be noted that all the results are obtained at the steady state and confirmed by stochastic simulation algorithm. In order to calculate mean first passage time, we provide a method using Fokker-Planck equation in an open-loop setting to obtain the drift and diffusion. Multiplicative interactions between different components indicate that it is possible to have cross-correlation between components. Most of the previous studies have focused on identifying the effect of cross-correlations and paid less attention to the formulation of the correlation strength analytically. Using our methodology and taking into account the classical definition of the cross-correlation between different noises, we are able to incorporate the cross-correlation effects into the total diffusion. We approximate the cross-correlation strength using the variances of the components. Mathematical formulation of the diffusion helps us investigate all possible modifications that can be introduced into the model, before designing the experiments. We provide stochastic

simulation algorithm to show that our formulation is in an excellent agreement with the results of the master equation.

In what follows, we demonstrate our method of noise decomposition and then, using the decomposed noise, we will decompose the induced correlation between components induced by different co-regulation processes into individual contributions. We imply our method to well-known sub-systems in gene regulation.

2.1 Noise decomposition

Our methodology relies on the decomposition of the total variability of a component in a network based on different sources of fluctuation. To this end, we use the corresponding equation for means, variances and co-variances of all components in a network obtained from the Fokker-Plank equation [44]. The decomposition indicates which reactions are responsible for high level of fluctuations in a network. We can easily compare the system's variability in the presence or absence of different components and system's modification in order to control the level of fluctuations. For example, in gene regulation, the presence or absence of processes like co-transcription, co-translation and addition of repressor to different parts of the system affect the level of fluctuation differently. Our method allows us to reconstruct biological networks by omitting or replacing some processes which cause high fluctuations.

Consider a general system of n dimension in which X represents the vector of all components. The components interact with each other through kinetic reactions sorted in a vector known as the reaction rate vector (also known as the propensity function) V . The length of V represents the number of reactions which occur in a system. The stoichiometry matrix S indicates which components and reactions are involved as reactants and products. In the stoichiometry matrix, rows correspond to specific components, and columns correspond to different reactions. Multiplication of the reaction rate vector and the stoichiometry matrix describes the macroscopic rate law of the system. Using linear noise approximation, one can write the time evolution of the corresponding mean vector \bar{X} and covariance matrix C as follows

$$\begin{cases} \dot{\bar{X}} = F(\bar{X}) = S.V, \\ \dot{C} = JC + CJ^T + B, \end{cases} \quad (2.1)$$

where $J = \frac{d}{dX}F(\bar{X})$ is the Jacobian matrix. Matrix B contains the internal

diffusion terms of all components and is given by

$$B = S \text{Diag}(V) S^T. \quad (2.2)$$

The steady state covariance matrix, which can be obtained by solving (2.1), contains both intrinsic and extrinsic fluctuations. Replacing the intrinsic variance of component i symbolically with

$$S_{Int}(i, i) = -\frac{B(i, i)}{\frac{\partial F_i}{\partial X_i} + \frac{\partial F_i}{\partial X_i}},$$

will help trace the effects of component i on other components' variability. From the fact that the covariance matrix C is a symmetric matrix ($C(i, j) = C(j, i)$), the covariance between components i and j can be written as follows

$$C(i, j) = -\frac{\sum_{\substack{k=1 \\ k \neq j}}^n \frac{\partial F_j}{\partial X_k} C(i, k) + \sum_{\substack{k=1 \\ k \neq i}}^n \frac{\partial F_i}{\partial X_k} C(j, k)}{\frac{\partial F_j}{\partial X_j} + \frac{\partial F_i}{\partial X_i}} + S_{Int}(i, j), \quad (2.3)$$

where $S_{Int}(i, j)$ is nonzero for $i = j$. By using (2.3), the normalized noise (coefficient of variation) induced from component i to component j will be

$$\eta^2(i, j) = \frac{dC(j, j)}{dS_{Int}(i, i)} \left(\frac{\bar{X}_i}{\bar{X}_j} \right)^2 \eta_{Int}^2(i),$$

where

$$\eta_{Int}^2(i) = \eta^2(i, i) = \frac{S_{Int}(i, i)}{\bar{X}_i^2},$$

denotes the intrinsic normalized noise of component i . Therefore, the total normalized noise induced to the component j can be written as

$$\eta_{total}^2(\bar{X}_j) = \sum_{i=1}^n \eta^2(i, j). \quad (2.4)$$

Noise decomposition helps us detect the components which make large contributions to the variability of specific components. It should be noted that all the results are obtained with the steady state assumptions. In the following, we apply the proposed method of noise decomposition to several well-known biological sub-systems.

2.1.1 Example - Translational regulation

Consider a protein which is translated by RNA and decays linearly in monostable system; RNA is transcribed at a constant rate and has a linear decay. The corresponding equations for the mean vector X and the covariance matrix C are given by equations (2.1) in which

$$X = \begin{bmatrix} R \\ P \end{bmatrix}, \quad S = \begin{bmatrix} 1 & -1 & 0 & 0 \\ 0 & 0 & 1 & -1 \end{bmatrix}, \quad V = \begin{bmatrix} \alpha \\ \gamma_R R \\ \lambda R \\ \gamma_P P \end{bmatrix},$$

denote the mean vector, stoichiometry matrix and reaction rates vector, respectively, and

$$C = \begin{bmatrix} C_{RR} & C_{RP} \\ C_{RP} & C_{PP} \end{bmatrix}, \quad J = \begin{bmatrix} -\gamma_R & 0 \\ \lambda & -\gamma_P \end{bmatrix}, \quad B = \begin{bmatrix} 2\gamma_R R & 0 \\ 0 & 2\gamma_P P \end{bmatrix},$$

represent covariance, Jacobian and diffusion matrices, respectively. The total normalized noise to the level of protein will be decomposed using (2.4) into the contributions of intrinsic and extrinsic fluctuations

$$\eta_{total}^2(P) = \underbrace{\eta_{Int}^2(P)}_{\eta^2(P,P)} + \underbrace{\frac{\tau_A}{\tau_R + \tau_A} \eta_{Int}^2(R)}_{\eta^2(R,P)},$$

where

$$\eta_{Int}^2(P) = \frac{1}{P},$$

$$\eta_{Int}^2(R) = \frac{1}{R}.$$

τ_i represents the half-life of component i . Although highly irregular behavior of RNA due to the low copy number can potentially affect the protein level, the variability from transcriptional burst may fade away and limit its effect on the regulation level because of the long life-time and stability of proteins. Kuwahara et al. [25] showed that the variability from transcriptional burst can substantially increase the mean of RNA and consequently the level of protein. They suggested that the increase in the steady state level can be created by the asynchronous nature of molecular reactions.

2.1.2 Example - Transcriptional regulation

System's modification by adding or omitting different components can substantially affect the variability of a system. Consider a three-dimensional open system (monostable) including a transcription factor P regulating the activity of the promoter A ; RNA production is regulated by the promoter, and all components decay through linear processes. The corresponding equations for the mean vector and covariance matrix are given by equations (2.1) in which

$$X = \begin{bmatrix} P \\ A \\ R \end{bmatrix}, \quad C = \begin{bmatrix} C_{PP} & C_{PA} & C_{PR} \\ C_{PA} & C_{AA} & C_{AR} \\ C_{PR} & C_{AR} & C_{RR} \end{bmatrix},$$

are the mean vector and covariance matrix and

$$S = \begin{bmatrix} 1 & -1 & 0 & 0 & 0 & 0 \\ 0 & 0 & 1 & -1 & 0 & 0 \\ 0 & 0 & 0 & 0 & 1 & -1 \end{bmatrix}, \quad V = \begin{bmatrix} \lambda \\ \gamma_P P \\ k_{on} P(1-A) \\ k_{off} A \\ v_m A \\ \gamma_R R \end{bmatrix},$$

represent the stoichiometry matrix and rate vector. Additionally

$$J = \begin{bmatrix} -\gamma_P & 0 & 0 \\ k_{on} & -(k_{off} + k_{on}) & 0 \\ 0 & v_m & -\gamma_R \end{bmatrix}, \quad B = \begin{bmatrix} 2\gamma_P P & 0 & 0 \\ 0 & 2k_{off} A & 0 \\ 0 & 0 & 2\gamma_R R \end{bmatrix},$$

denote the Jacobian and diffusion matrices, respectively. By using the same strategy as shown in the previous example, we can decompose the total normalized noise to the level of RNA into intrinsic and extrinsic noise

$$\begin{aligned} \eta_{total}^2(R) &= \underbrace{\eta_{Int}^2(R)}_{\eta^2(R,R)} + \underbrace{\frac{\tau_A}{\tau_R + \tau_A} \eta_{Int}^2(A)}_{\eta^2(A,R)} \\ &+ \underbrace{\frac{\tau_P}{\tau_A + \tau_P} \frac{\tau_A}{\tau_A + \tau_R} \frac{\tau_A (\tau_P \tau_R + \tau_A \tau_R + \tau_A \tau_P)}{\tau_R + \tau_P} \eta_{Int}^2(P)}_{\eta^2(P,R)}, \end{aligned} \tag{2.5}$$

where τ_i represents the half-life of component i and $K_D = \frac{k_{off}}{k_{on}}$, and

$$\begin{aligned}\eta_{Int}^2(P) &= \frac{1}{P}, \\ \eta_{Int}^2(A) &= \frac{K_D}{P}, \\ \eta_{Int}^2(R) &= \frac{1}{R},\end{aligned}\tag{2.6}$$

are the intrinsic normalized noises. Equation (2.5) shows how different parameters regulate the RNA fluctuation level. For example, longer half-lives of the components increase the variability to the level of RNA while high concentrations of components reduce the RNA variability.

2.1.3 Example - RNA enzymatic decay

In the previous example, the transcription factor P was involved in RNA production. This introduces a positive correlation between the protein and RNA. There are possibilities in which some components are involved in other components' decay process. In this example, we show that although the correlation between such components is negative, the effect on normalized noise is positive. We consider the system in the previous example and introduce an enzymatic decay to RNA in which the corresponding enzyme is a Poisson process. We regulate the system's parameters in a way that the level of RNA and consequently the intrinsic noise does not change. Therefore, the corresponding equations for the mean vector and covariance matrix are given by equations (2.1) in which

$$X = \begin{bmatrix} P \\ A \\ E \\ R \end{bmatrix}, \quad C = \begin{bmatrix} C_{PP} & C_{PA} & C_{PE} & C_{PR} \\ C_{PA} & C_{AA} & C_{AE} & C_{AR} \\ C_{PE} & C_{AE} & C_{EE} & C_{ER} \\ C_{PR} & C_{AR} & C_{ER} & C_{RR} \end{bmatrix},\tag{2.7}$$

and

$$S = \begin{bmatrix} 1 & -1 & 0 & 0 & 0 & 0 & 0 & 0 \\ 0 & 0 & 1 & -1 & 0 & 0 & 0 & 0 \\ 0 & 0 & 0 & 0 & 1 & -1 & 0 & 0 \\ 0 & 0 & 0 & 0 & 0 & 0 & 1 & -1 \end{bmatrix}, \quad V = \begin{bmatrix} \lambda \\ \gamma_P P \\ k_{on} P(1 - A) \\ k_{off} A \\ v_m A \\ \alpha \\ \gamma_E E \\ \gamma_R R \end{bmatrix},$$

$$J = \begin{bmatrix} -\gamma_P & 0 & 0 & 0 \\ k_{on} & -(k_{off} + k_{on}) & 0 & 0 \\ 0 & 0 & -\gamma_E & 0 \\ 0 & v_m & -\gamma_R R & -\gamma_R E \end{bmatrix}, \quad B = \begin{bmatrix} 2\gamma_P P & 0 & 0 & 0 \\ 0 & 2k_{off} A & 0 & 0 \\ 0 & 0 & 2\gamma_E E & 0 \\ 0 & 0 & 0 & 2\gamma_R R \end{bmatrix}.$$

The total normalized noise to the level of protein can be decomposed using (2.3) into the contribution of different sources of stochasticity as follows

$$\begin{aligned} \eta_{total}^2(R) &= \underbrace{\eta_{Int}^2(R)}_{\eta^2(R,R)} + \underbrace{\frac{\tau_E}{\tau_R + \tau_E} \eta_{Int}^2(E)}_{\eta^2(E,R)} + \underbrace{\frac{\tau_A}{\tau_R + \tau_A} \eta_{Int}^2(A)}_{\eta^2(A,R)} \\ &+ \underbrace{\frac{\tau_P}{\tau_A + \tau_P} \frac{\tau_A}{\tau_A + \tau_R} \frac{\tau_A (\tau_P \tau_R + \tau_A \tau_R + \tau_A \tau_P)}{\tau_R + \tau_P}}_{\eta^2(P,R)} \eta_{Int}^2(P), \end{aligned} \quad (2.8)$$

where τ_E is the enzyme half-life and

$$\eta_{Int}^2(E) = \frac{1}{E}.$$

Small changes in the level of enzymes make a considerable change in the normalized noise of RNA. This shows that the extrinsic fluctuations from decay processes are substantial sources of randomness in stochastic modeling and can be controlled by changing specific parameters. Noise decomposition helps to analytically predict and prevent undesirable behaviors in a system by modifying the reactions which propagate the noise through a network. High order reactions in a network can introduce a cross-correlation between components which can affect the level of expectation values. These effects are not trivial and cannot be captured by traditional methods [45, 46].

2.2 Co-regulation processes

In biological networks, it is common to have correlation between identical components due to co-regulation processes. There might be several co-regulation processes that connect two components. It is important to investigate how different processes are related and determine the strength of individual correlations induced by each process, and also control the key parameters which affect the strength of such correlations. For example, two identical RNAs can be correlated by being decayed by the same enzyme and/or be regulated by the same promoter. It is interesting to investigate whether there is a connection between these co-regulation processes.

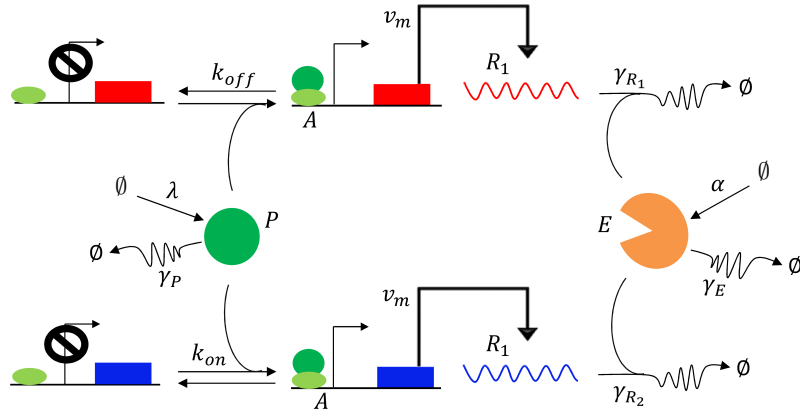


Figure 2.1: Co-regulation processes. R_1 and R_2 are two identical RNAs which are degraded by the same enzyme E and their promoters are regulated by the same transcription factor P .

Suppose that \bar{X}_i and \bar{X}_j are identical components in a network which have the same level of total normalized noises, and the component κ coregulates \bar{X}_i and \bar{X}_j by a specific co-regulation process. The extrinsic noises $\eta(\kappa, \bar{X}_i)$ induced by component κ to the level of \bar{X}_i and \bar{X}_j are equal and can be calculated using equation (2.3). The corresponding correlation coefficient to a specific co-regulation process will be given by

$$\rho_{\kappa}(\bar{X}_i, \bar{X}_j) = \frac{\eta(\kappa, \bar{X}_i)}{\eta_{total}(\bar{X}_i)} = \frac{\eta(\kappa, \bar{X}_j)}{\eta_{total}(\bar{X}_j)}. \quad (2.9)$$

In the presence of different co-regulation processes, the total correlation between two identical components regulated by such processes is simply the summation of individual correlations

$$\rho_{total}(\bar{X}_i, \bar{X}_j) = \sum_{t=1}^m \rho_{\kappa_t}(\bar{X}_i, \bar{X}_j) = \sum_{t=1}^m \frac{\eta(\kappa_t, \bar{X}_i)}{\eta_{total}(\bar{X}_i)}. \quad (2.10)$$

Decomposition of correlation induced by co-regulation processes helps us reconstruct a system with more desirable processes. In the following example we decompose the correlation between two RNAs induced by different co-regulation processes.

2.2.1 Example - Co-regulation processes

Consider the previous example (2.1.3) in which a transcription factor regulates promoter activation; the promoter regulates the RNA production; and the enzyme is involved in RNA degradation. In addition, we add a second RNA which

is identical to the first RNA and suppose that the promoter of the second RNA is regulated by the same transcription factor and being degraded by the same enzyme (Figure 2.1). The enzymatic decay and co-transcriptional regulation are the co-regulation processes that connect the two RNAs. From (2.9), the correlation between the two RNAs can be decomposed into the contributions of co-regulation processes as follows

$$\rho(R_1, R_2) = \rho_E(R_1, R_2) + \rho_P(R_1, R_2),$$

where

$$\rho_E(R_1, R_2) = \frac{\eta^2(E, R)}{\eta_{total}^2(R)}, \quad \rho_P(R_1, R_2) = \frac{\eta^2(P, R)}{\eta_{total}^2(R)},$$

are the correlations induced by the enzymatic decay and co-transcriptional regulation processes. The extrinsic normalized noises $\eta^2(P, R)$, $\eta^2(E, R)$ and $\eta_{total}^2(R)$ have been defined in the previous example. Although the induced correlation by the co-transcriptional process does not affect the correlation induced by the enzymatic decay and vice versa, variations in the value of a shared parameter can regulate both correlations.

2.3 Mean first passage time (MFPT)

Mean first passage time (MFPT), the average time for a random variable to switch from one steady state to another, can be interpreted as the cellular memory which is a ubiquitous phenomenon in biology. The most common method for calculation of MFPT uses the Fokker-Plank equation (1.9) which results in

$$H(x) \frac{d}{dx} T(x) + \frac{1}{2} D_{total}(x) \frac{\partial^2}{\partial x^2} T(x) = -1, \quad (2.11)$$

with the boundary conditions

$$T(R) = 0, \quad \frac{d}{dx} T(x) |_{x=R^*} = 0. \quad (2.12)$$

$H(x)$ and $D_{total}(x)$ represent the drift and diffusion, respectively, and $T(x)$ is the MFPT. In the absence of stochasticity, the potential function is given by

$$V(x) = - \int H(x) dx.$$

The stationary solution of the vector field $H(x)$ corresponds to a delta distribution at the extremum of $V(x)$. The diffusion, $D_{total}(x)$, which is often

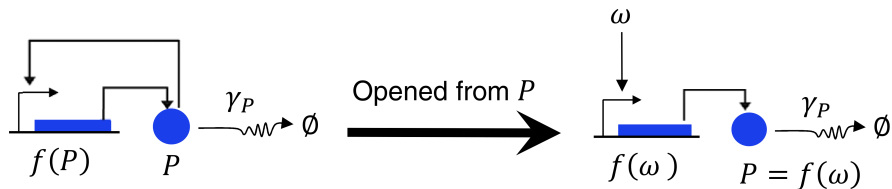


Figure 2.2: A single-component feedback system in which a protein regulates its promoter cooperatively, described by a Hill-function $f(P)$ with the Hill-coefficient $n = 2$. The closed-loop system (left) is opened at the protein level (right).

characterized with a considerable uncertainty, smoothens the distribution by creating tails which determine the escape probability from one potential well to another. In order to investigate the MFPT, we address the issue of how to define the diffusion $D_{total}(x)$.

2.3.1 Example - Feedback loop system with a single component

As a very simple example, consider a feedback loop with a single component, which regulates its own production (Figure 2.2). The closed feedback loop is described by the following ordinary differential equation (ODE)

$$\frac{d}{dt}P = b + v_m \frac{P^n}{K_D^n + P^n} - \gamma_P P, \quad (2.13)$$

in which K_d denotes the equilibrium dissociation constant, b and v_m are the basal and maximum production rates and γ_P stands for the decay rate constant of the protein. The index of cooperativity, the Hill number, is denoted by n and is taken to be two for all calculations. In all our examples, the parameters have no physical dimension, but their values are representative for yeast when the time and concentration units are expressed in hours and nM . System (2.13) indicates that all the fluctuations are intrinsic. Therefore, the drift can be calculated from the Ito interpretation (1.6) and the diffusion can be calculated based on equation (2.2)

$$\begin{aligned} H(P) &= b + v_m \frac{P^n}{K_D^n + P^n} - \gamma_P P, \\ D_{total}(P) &= b + v_m \frac{P^n}{K_D^n + P^n} + \gamma_P P. \end{aligned} \quad (2.14)$$

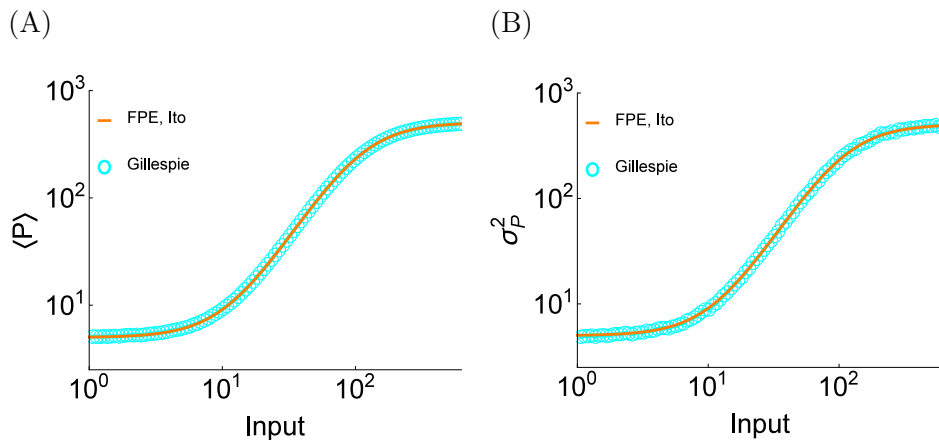


Figure 2.3: A single-component system comprising protein. The mean (A) and the variance (B) of the open-loop output with respect to the input are obtained from the stochastic simulation algorithm (cyan circle) and the analytical approach (orange solid). The following parameters are fixed: $K_D = 110$, $v_m = 500$, $b = \frac{v_m}{100}$, $\gamma_P = 1$.

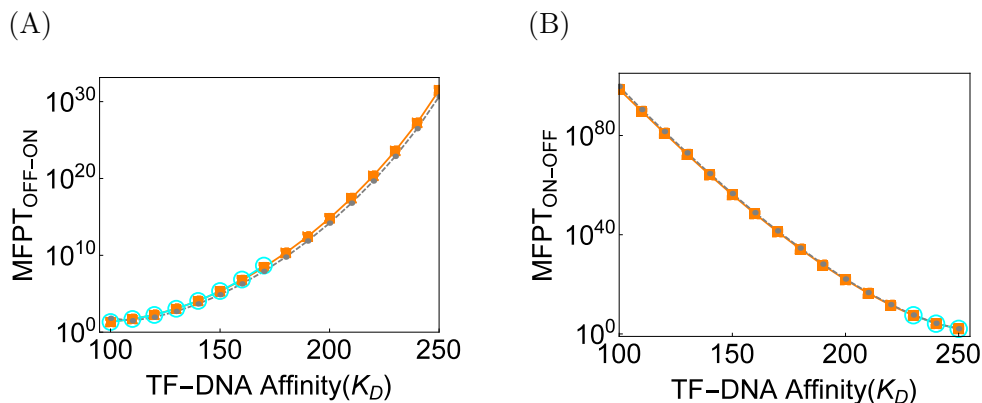


Figure 2.4: A single-component feedback system comprising protein. (A) Mean first passage time (MFPT) from the OFF to the ON state and (B) from the ON to OFF state were calculated for the bistable range of the K_D . The good agreement between the stochastic simulation algorithm (cyan circle) and the analytical approach (orange rectangle) indicates the accuracy of the method. With the obtained drift and diffusion, MFPT was also calculated using the Kramers method (1.18) (gray dashed). The following parameters are fixed: $v_m = 500$, $b = \frac{v_m}{100}$, $\gamma_P = 1$.

With the above equations, equation (2.11) together with the boundary condition (2.12) can be used to calculate MFPT. Figure 2.4 shows that there is an agreement between the results of stochastic simulation algorithm (cyan circle) and that of our theoretical approach (orange rectangle) which indicates the accuracy

of the method. The gray dashed curve represents the Kramers approximation and indicates the accuracy of this method provided that we have accurate drift and diffusion.

2.4 Characterization of drift by the open-loop approach

In the study of complex networks in which a huge number of components interact with each other, the quasi steady state assumption can reduce the dimension of the system. The quantitative characterization of positive feedback loops has been facilitated by system reduction. An efficient method for system reduction is termed the open-loop approach [1], which can be used to determine whether a positive feedback loop system displays bistability. By opening the feedback loop, a feedback component is broken into a pair of input and output. The mapping of the input into the output defines a single variable open-loop function, which contains all essential information on bistability without the need to analyze the complicated closed-loop system with multiple variables. If the open-loop function is sigmoidal, then the feedback loop has the potential to display bistability. This deterministically formulated open-loop approach has important applications [1, 31, 39]. Experimentally, the open-loop response can be measured to determine whether a multicomponent feedback gene network can display bistability, without knowing any details on the reactions in the feedback loop. In theoretical analysis, the open-loop approach can be used to determine the maximal bistable range of a single parameter in a multidimensional parameter space. The open-loop function, $\eta = f(\omega)$, assigns to each value of the input ω an output value η . Intersections of $\eta = f(\omega)$ with the identity line $\eta = \omega$ (black line, Figure 2.5, left) represent the steady states for the closed-loop system. When there are three intersections, the system is bistable (Figure 2.5, right). The upper and lower stable steady states are denoted by “ON” and “OFF” states. The open-loop function can be used to represent the drift. In a feedback loop system with single variable, there is only one way of opening the loop (Figure 2.3). While the opening can be performed at any variable for the deterministic characterization, this is not the case for stochastic calculations. Since only the fast variable can be considered to be in equilibrium, the loop has to be opened at the slowest variable which we are interested to obtain its MFPT. The output is affected directly by intrinsic fluctuations and also indirectly by the fluctuations of all components in the loop that are propagated to the output. Therefore, the diffusion has to be re-defined for the single variable open-loop output that

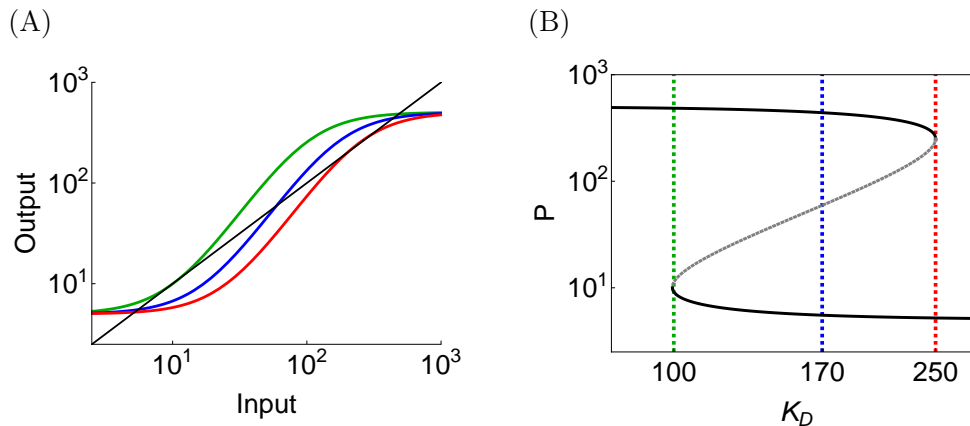


Figure 2.5: Steady states of a one-component system presented in open-loop (A) and closed-loop (B) versions. The open-loop response is shown for $K_D = 100$ (red) and $K_D = 220$ (blue). The corresponding steady-state values in the closed-loop system are indicated by dashed lines of the same color. The following parameters are fixed: $v_m = 500$, $b = \frac{v_m}{100}$, $\gamma_P = 1$.

reproduces the effect of fluctuations due to all components in the original system. Although the open-loop function contains all the information about the nonlinearity that determines the number and the level of the steady-states, it does not have to reflect any physical parameter separately. To predict transition rates, all relevant parameters have to be specified, in particular the time scale of the broken component. The open-loop function reduces a multivariable system to a one-variable function. Similarly, the diffusion matrix has to be reduced.

2.5 Calculation of diffusion with uncorrelated white noises

Equation (2.11), used to calculate the MFPT, is typically applied to one-dimensional systems. However, most biologically realistic feedback loops contain multiple components. In order to obtain the total diffusion induced to specific components in a multidimensional system, we use equations (2.1) provided that the sources of fluctuation are independent. This indicates that the drift is independent of the fluctuation and the Ito interpretation is used. Therefore, the steady-state mean values of all variables are identical to their deterministic values. It is important to emphasize that the LNA is applied to the open-loop system. For closed-loop bistable systems, the LNA can be used only locally, around the steady-states and not globally while it can be used at all values of the input of the open-loop system. It is common in biological networks that

some components have considerably shorter life times compared to the other parts. Existence of unobservable configurations in a system may lead to significant numerical stiffness. Elimination of fast components (by applying the quasi-steady-state assumption) [21, 49] can reduce the complexity of the calculation as well as stiffness. Invoking timescale separation conditions can divide systems of equations (2.1) into two sub systems which represent the mean of fast and slow variables

$$\frac{d}{dt}X_f = H_f, \quad \frac{d}{dt}X_s = H_s, \quad (2.15)$$

and their variances

$$\begin{aligned} \frac{d}{dt}C_{ff} &= J_f C_{ff} + (J_f C_{ff})^T + B_f, \\ \frac{d}{dt}C_{sf} &= (J_f + J_s) C_{sf} + \left(J_s^f C_{ff}\right)^T, \\ \frac{d}{dt}C_{ss} &= J_s C_{ss} + (J_s C_{ss})^T + J_s^f C_{sf} + \left(J_s^f C_{sf}\right)^T + B_s. \end{aligned} \quad (2.16)$$

The indices s and f stand for the slow and fast components, respectively. The covariance, Jacobian and diffusion matrices are presented by fast and slow sub-matrices

$$C = \begin{bmatrix} C_{ff} & C_{sf} \\ C_{sf} & C_{ss} \end{bmatrix}, \quad J = \begin{bmatrix} J_f^f & J_f^s \\ J_s^f & J_s^s \end{bmatrix}, \quad B = \begin{bmatrix} B_f & 0 \\ 0 & B_s \end{bmatrix}, \quad (2.17)$$

where $C_{ii} = \text{var}(X_i)$ and $C_{ij} = \text{cov}(X_i, X_j)$, and

$$J_i^j = \frac{\partial}{\partial X_j} (H_i(X)). \quad (2.18)$$

Applying the quasi-steady state assumption to systems (2.15) and (2.16) for the fast component leads to the following slow sub-systems with a single slow variable

$$\begin{aligned} \frac{d}{dt}\bar{X}_s &= H_s(\bar{X}_s), \\ \frac{d}{dt}\bar{C}_{ss} &= J_s \bar{C}_{ss} + \bar{C}_{ss} J_s^T + D_{total}, \end{aligned} \quad (2.19)$$

where

$$D_{total} = \underbrace{B_s}_{D_{Intrinsic}} + \underbrace{J_s^f \left(J_f^f + J_s^s \right)^{-1} B_f \left(\left(J_f^f \right)^T \right)^{-1} \left(J_f^f \right)^T}_{D_{Extrinsic}}, \quad (2.20)$$

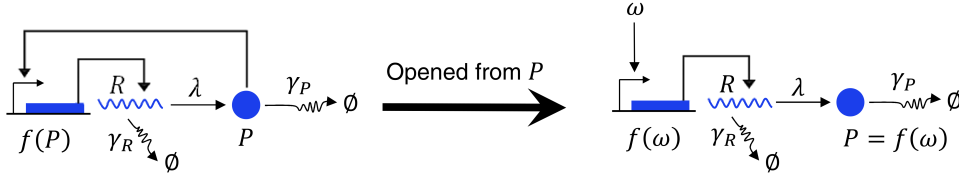


Figure 2.6: A two-component system consisting of an RNA and a protein. The closed-loop system (left) is opened at the protein level (right).

provided that fast components are uncoupled. For the sake of recognizing the reduced system from the original system, we use the variables \bar{X}_s and \bar{C}_{ss} for the reduced system. The total diffusion D_{total} for the slow variable \bar{X}_s is the summation of the intrinsic diffusion ($D_{Intrinsic}$) and the diffusion induced by the fast variables ($D_{Extrinsic}$). With the total diffusion D_{total} and drift $H_s(\bar{X}_s)$, we can calculate the MFPT from equation (2.11) with proper boundary conditions.

2.5.1 Example - Positive feedback loop system comprising RNA and protein

Consider a two-dimensional feedback loop system in which a protein (P) regulates transcription, an RNA (R) regulates the translation, and both components have linear decays (Figure 2.6)

$$\begin{aligned} \frac{d}{dt}R &= b + v_m \frac{P^2}{K_D^2 + P^2} - \gamma_R R \\ \frac{d}{dt}P &= \lambda R - \gamma_P P. \end{aligned} \quad (2.21)$$

The translation and RNA decay rates are tuned so that the open-loop function is identical to that of previous example. Consequently, the bistable ranges of K_d are also identical in the feedback loop systems. By opening the feedback loop, the part of the protein that regulates the RNA becomes the input ω , and P becomes the output

$$\begin{aligned} \frac{d}{dt}R &= b + v_m \frac{\omega^2}{K_D^2 + \omega^2} - \gamma_R R, \\ \frac{d}{dt}P &= \lambda R - \gamma_P P. \end{aligned} \quad (2.22)$$

The output is then produced under the control of the input and unable to regulate the RNA (Figure 2.6). The corresponding time evolution of the covariance

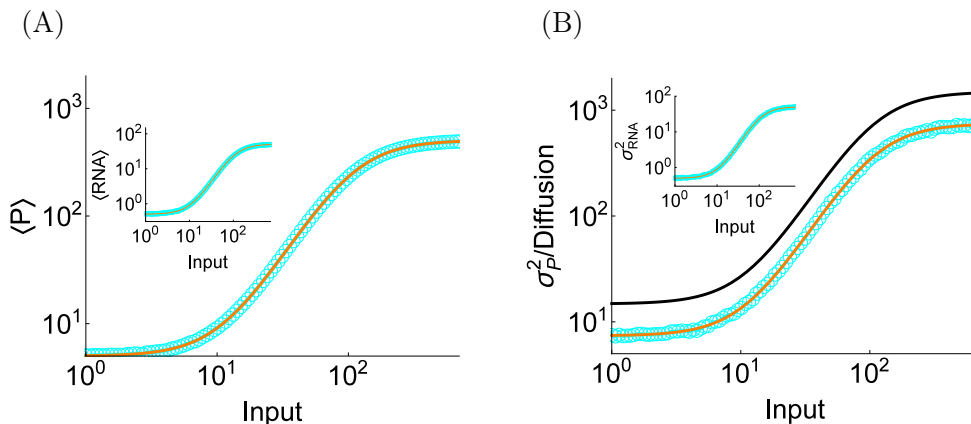


Figure 2.7: A two-component system consisting of an RNA and a protein. (A) The mean and (B) the variance of the output with respect to the input is calculated by using stochastic simulation algorithm (cyan circle) and analytical approach (orange solid). Mean and variance of RNA are shown in the inset. The following parameters are fixed: $K_D = 110$, $v_m = 1000$, $b = \frac{v_m}{100}$, $\gamma_{RNA} = 20$, $\gamma_P = 1$, $\lambda = 10$.

matrix to system (2.22) can be obtained from (2.1) in which

$$X = \begin{bmatrix} R \\ P \end{bmatrix}, \quad C = \begin{bmatrix} C_{RR} & C_{RP} \\ C_{RP} & C_{PP} \end{bmatrix},$$

are the mean vector and covariance matrix, and

$$J = \begin{bmatrix} -\gamma_R & 0 \\ \lambda & -\gamma_P \end{bmatrix}, \quad B = \begin{bmatrix} b + v_m \frac{\omega^2}{K_D^2 + \omega^2} + \gamma_R R & 0 \\ 0 & \lambda R + \gamma_P P \end{bmatrix},$$

are Jacobian and diffusion (based on (2.2)) matrices, respectively. The life time of RNA is considerably shorter than that of the protein and therefore it can be taken as the fast variable. Since system (2.22) contains only first order reactions, the Ito method is applied. Applying the quasi-steady state assumption to system (2.22) and the time evolution of its corresponding covariance matrix, one gets the following reduced system

$$\begin{aligned} \frac{d}{dt} \bar{P} &= \frac{\lambda}{\gamma_R} \left(b + v_m \frac{\omega^2}{K_D^2 + \omega^2} \right) - \gamma_P \bar{P}, \\ \frac{d}{dt} \bar{C}_{PP} &= -2\gamma_P \bar{C}_{PP} + D_{total}, \end{aligned} \tag{2.23}$$

in which the total diffusion to the level of protein can be obtained from equa-

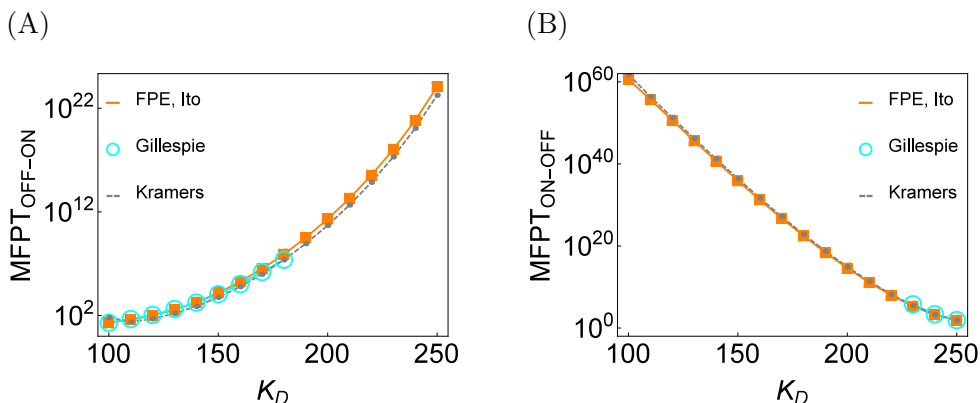


Figure 2.8: A two-component system consisting of an RNA and a protein. (A) MFPT from OFF to ON state and (B) from ON to OFF state are calculated for the bistable range of K_D . MFPT is also calculated using the Kramers method (1.18) (gray dashed). The following parameters are fixed: $v_m = 1000$, $b = \frac{v_m}{100}$, $\gamma_{RNA} = 20$, $\gamma_P = 1$, $\lambda = 10$.

tion (2.20)

$$\begin{aligned}
 D_{total} = & \underbrace{\frac{\lambda}{\gamma_R} \left(b + v_m \frac{\omega^2}{K_D^2 + \omega^2} \right)}_{D_{Intrinsic}} + \gamma_P \bar{P} \\
 & + 2 \underbrace{\frac{\lambda^2}{\gamma_R^2 (\gamma_R + \gamma_P)} \left(b + v_m \frac{\omega^2}{K_D^2 + \omega^2} \right)}_{D_{Extrinsic}}.
 \end{aligned} \tag{2.24}$$

Figure 2.7 shows the accuracy of the diffusion term (2.24). In order to calculate the MFPT, we need to re-close the loop to recreate the multistable system. With the drift and diffusion from (2.24) and (2.23), we can calculate MFPT from equation (2.11) with the boundary condition (2.12) for different parameter values. The MFPT is calculated for the entire bistable range of K_d . The OFF \rightarrow ON transitions are fast at the lower bistable boundary and increase by increasing K_d . The MFPT was less for the two-variable system than for the one-variable system because the RNA, varying between 0.5 and 50, introduces low concentrations and large noise into the two-variable system although in both systems, the protein concentration varies between 5 and 500 nM . To validate our prediction, we compared the MFPT obtained from the Fokker-Plank equation to the one calculated by the stochastic simulation algorithm (SSA). The results show that there is a very good agreement between the two calculation (Figure 2.8). We calculated the MFPT up to 10^5 hours, which corresponds to the upper limit of experimentally realistic time-scale, i.e.

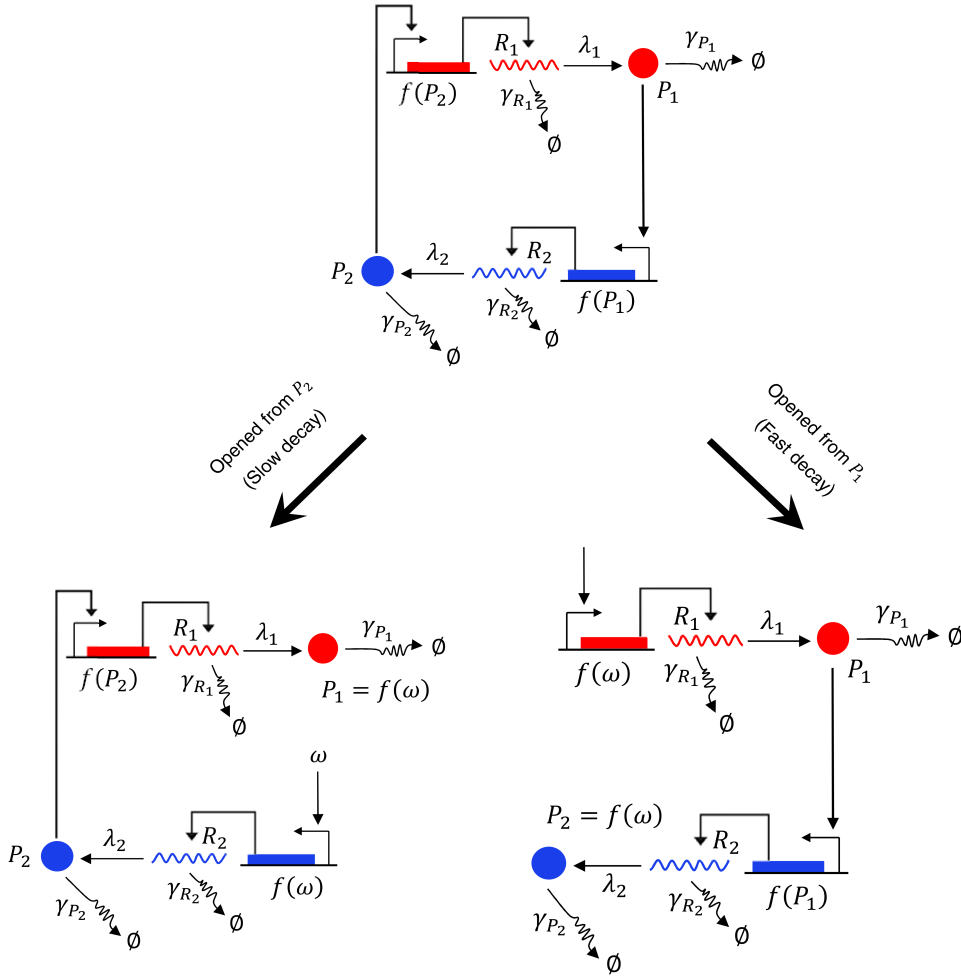


Figure 2.9: A four-component system consisting of two RNAs and two proteins. The closed-loop system (top) is opened either at P_1 with the shorter half-life (right) or at P_2 with the longer half-life (left). In the closed-loop system, P_2 regulates the transcription of R_1 and P_1 regulates the transcription of R_2 cooperatively, with a Hill-coefficient of $n = 2$ at each promoter.

11 years. We have also checked the prediction of the MFPT by Kramers formula (1.18), which was also in good agreement with the SSA.

2.5.2 Example - Opening the loop at the slowest components is necessary in MFPT calculation

Opening the feedback loop from different components may not yield the same results for the MFPT when using the analytical approach and the SSA. In the following example, we explore a double activator feedback system, in which the two proteins activate each other's transcription. One of the proteins (P_1) has a five-time faster decay rate than the other (Figure 2.9). The translation rate

constants are adjusted so that the maximum concentrations for both proteins are equal. Since the RNAs encoding for the two different proteins are explicitly modeled, we have the following four-dimensional system.

$$\begin{aligned}\frac{d}{dt}R_1 &= f(P_2) - \gamma_R R_1, \\ \frac{d}{dt}P_1 &= \lambda_1 R_1 - \gamma_{P_1} P_1, \\ \frac{d}{dt}R_2 &= f(P_1) - \gamma_R R_2, \\ \frac{d}{dt}P_2 &= \lambda_2 R_2 - \gamma_P P_2,\end{aligned}\tag{2.25}$$

where

$$f(P_i) = b + v_m \frac{P_i^2}{K_D^2 + P_i^2}.\tag{2.26}$$

The covariance matrix will be extended to the corresponding enzyme

$$\frac{d}{dt}C = J C + (J C)^T + B,\tag{2.27}$$

where

$$X = \begin{bmatrix} R_1 \\ P_1 \\ R_2 \\ P_2 \end{bmatrix}, \quad C = \begin{bmatrix} C_{R_1 R_1} & C_{R_1 P_1} & C_{R_1 R_2} & C_{R_1 P_2} \\ C_{R_1 R_2} & C_{P_1 P_1} & C_{P_1 R_2} & C_{P_1 P_2} \\ C_{R_2 R_2} & C_{R_1 P_2} & C_{P_1 P_2} & C_{R_2 P_2} \\ C_{R_1 P_2} & C_{P_1 P_2} & C_{R_2 P_2} & C_{P_2 P_2} \end{bmatrix},$$

are the mean vector and covariance matrix, and

$$J = \begin{bmatrix} -\gamma_R & 0 & 0 & 0 \\ 0 & -\gamma_{P_1} + J_{\eta_1} & 0 & 0 \\ 0 & 0 & -\gamma_R & 0 \\ 0 & 0 & 0 & -\gamma_{P_2} + J_{\eta_2} \end{bmatrix},$$

represents the Jacobian matrix. Additionally,

$$B = \begin{bmatrix} f(P_1) + \gamma_R R_1 & 0 & 0 & 0 \\ 0 & \lambda_1 R_1 + \gamma_{P_1} P_1 & 0 & 0 \\ 0 & 0 & f(P_2) + \gamma_R R_2 & 0 \\ 0 & 0 & 0 & \lambda_2 R_2 + \gamma_P P_2 \end{bmatrix},$$

denotes the diffusion matrix. To illustrate the importance of the choice where to open the loop, we open the feedback once at P_1 , that is, at the level of the protein with the fast decay rate, and another time at P_2 , which is the protein

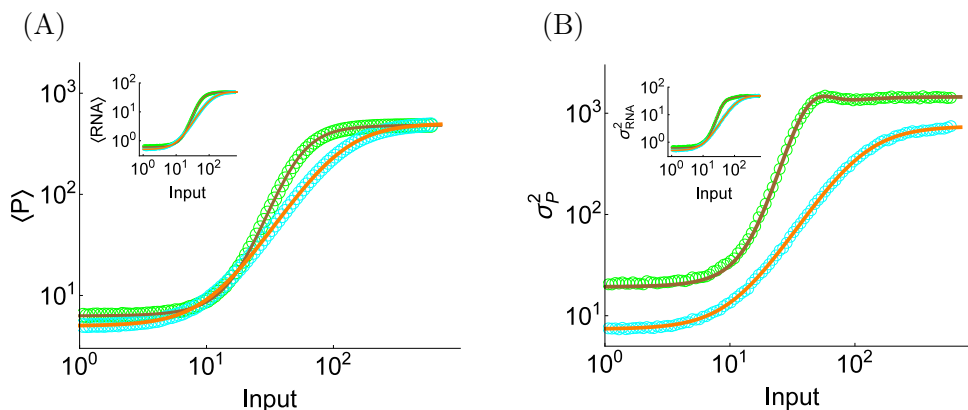


Figure 2.10: A four-component system consisting of two RNAs and two proteins. The feedback loop is opened at P_1 . (A) The mean and (B) variance of the output is calculated by the stochastic simulation algorithm for P_1 (green circle) and P_2 (cyan circle) and by the analytical approach (brown and orange solid, respectively). Means and variances for RNAs are shown in the inset. The following parameters are fixed: $K_D = 110$, $v_m = 1000$, $b = \frac{v_m}{100}$, $\gamma_{R_1} = \gamma_{R_2} = 20$, $\gamma_{P_1} = 5$, $\gamma_{P_2} = 1$, $\lambda_1 = 50$, $\lambda_2 = 10$.

with the slow decay rate. Opening from a protein P_j results in

$$J_{\eta_j} = 0, \quad J_{\eta_i} = \frac{d}{dP_i} f(P_i).$$

The life time of RNAs are considerably shorter than proteins and therefore RNAs can be taken as the fast variables and put at the steady state. By opening the feedback at P_j , P_i ($i \neq j$) should be taken at the steady state. Since the open-loop system contains nonlinearities, the Stratonovich interpretation is applied (see Section 1.2.3). In this example, we show that in a system in which nonlinearity is caused by only one component, there is no cross-correlation between sources of fluctuation. Applying the quasi-steady state assumption, systems (2.25) and (2.27) are reduced to the following system provided that the feedback loop is opened at P_j

$$\begin{aligned} \frac{d}{dt} \bar{P}_j &= H(P_j), \\ \frac{d}{dt} \bar{C}_{P_j P_j} &= -2\gamma_{P_j} \bar{C}_{P_j P_j} + D_{total}, \end{aligned} \tag{2.28}$$

where according to (2.20), the total diffusion to the level of protein will be

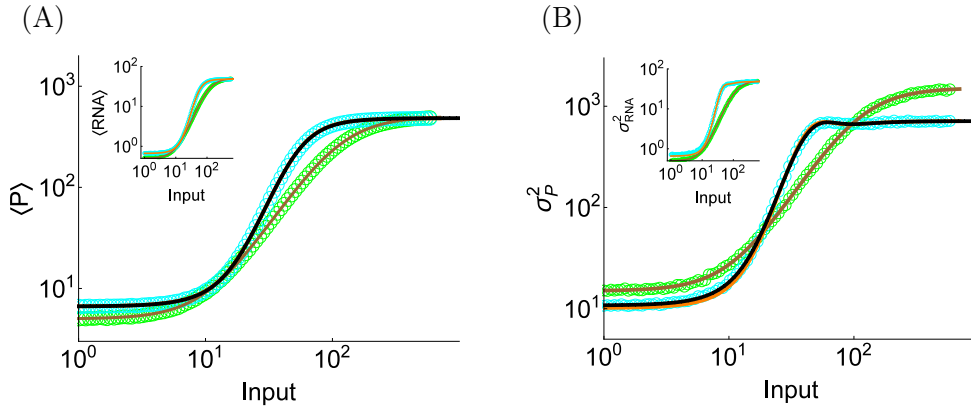


Figure 2.11: A four-component system consisting of two RNAs and two proteins. The feedback loop is opened at P_2 . (A) The mean and (B) variance of the output is calculated by the stochastic simulation algorithm for P_1 (green circle) and P_2 (cyan circle) and by the analytical approach (brown and orange solid, respectively). Means and variances for RNAs are shown in the inset. The black dashed curves are functions fitted to mean and variance of P_2 (see 2.8.2). The following parameters are fixed: $K_D = 110$, $v_m = 1000$, $b = \frac{v_m}{100}$, $\gamma_{R_1} = \gamma_{R_2} = 20$, $\gamma_{P_1} = 5$, $\gamma_{P_2} = 1$, $\lambda_1 = 50$, $\lambda_2 = 10$.

$$\begin{aligned}
 D_{total}(\bar{P}_j) &= \underbrace{\frac{\lambda_j}{\gamma_R} \left(b + v_m \frac{\left(\frac{\lambda_j}{\gamma_{P_i} \gamma_R} f(\omega) \right)^2}{K_D^2 + \left(\frac{\lambda_j}{\gamma_{P_i} \gamma_R} f(\omega) \right)^2} \right)}_{D_{Intrinsic}} + \gamma_{P_j} \bar{P}_j \\
 &+ \underbrace{\frac{2\lambda_j^2 \lambda_i^2 v_m f(\omega)}{\gamma_{P_i} \gamma_R^2 (\gamma_R + \gamma_{P_j})^2 (\gamma_{P_i} + \gamma_{P_j})} \left(\frac{2v_m K_D^2 \lambda_j f(\omega)}{\gamma_{P_i} \gamma_R \left(K_D^2 + \left(\frac{\lambda_j}{\gamma_{P_i} \gamma_R} f(\omega) \right)^2 \right)^2} \right)^2}_{D_{Extrinsic(R_i \rightarrow P_j)}} \\
 &+ \underbrace{\frac{2\lambda_j^3 f(\omega)}{\gamma_{P_i} \gamma_R^2 (\gamma_R + \gamma_{P_j}) (\gamma_{P_i} + \gamma_{P_j})} \left(\frac{2v_m K_D^2 \lambda_j f(\omega)}{\gamma_{P_i} \gamma_R \left(K_D^2 + \left(\frac{\lambda_j}{\gamma_{P_i} \gamma_R} f(\omega) \right)^2 \right)^2} \right)^2}_{D_{Extrinsic(P_i \rightarrow P_j)}} \\
 &+ \underbrace{\frac{2\lambda_j^2}{\gamma_R (\gamma_R + \gamma_{P_j})} \left(b + v_m \frac{\left(\frac{\lambda_j}{\gamma_{P_1} \gamma_R} f(\omega) \right)^2}{K_D^2 + \left(\frac{\lambda_j}{\gamma_{P_1} \gamma_R} f(\omega) \right)^2} \right)}_{D_{Extrinsic(R_j \rightarrow P_j)}}.
 \end{aligned} \tag{2.29}$$

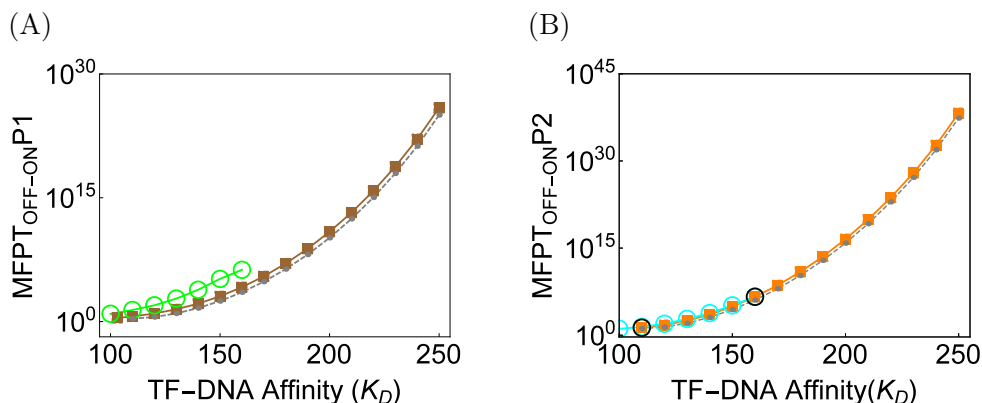


Figure 2.12: A four-component system consisting two RNAs and two proteins. The MFPT from OFF to ON state is calculated for (A) P_1 and (B) P_2 for the bistable range of K_D . A good agreement between the stochastic simulation algorithm and analytical approach for the opening at P_2 is observed in (B). The results in (A) illustrate that this is the case for the opening at P_1 . This indicates that in order to calculate the total diffusion, only variables that are faster than the input and output can be considered to be in steady-state. The black circles in (B) represent the MFPT values which are calculated using the drift and diffusion fitted to the open-loop data. The following parameters are fixed: $v_m = 1000$, $b = \frac{v_m}{100}$, $\gamma_{R_1} = \gamma_{R_2} = 20$, $\gamma_{P_1} = 5$, $\gamma_{P_2} = 1$, $\lambda_1 = 50$, $\lambda_2 = 10$.

and

$$\begin{aligned}
 H(P_j) = & \frac{\lambda_j}{\gamma_R} \left(b + v_m \frac{\left(\frac{\lambda_j}{\gamma_{P_i} \gamma_R} f(\omega) \right)^2}{K_D^2 + \left(\frac{\lambda_j}{\gamma_{P_i} \gamma_R} f(\omega) \right)^2} \right) - \gamma_{P_j} \bar{P}_j \\
 & + \frac{v_m^2 \lambda_j K_D^2 (\lambda_j + \gamma_R + \gamma_{P_i})}{\gamma_R^2 (\gamma_R + \gamma_{P_i})} \frac{\left(K_D^2 - 3 \left(\frac{v_m \lambda_i}{\gamma_R \gamma_{P_i}} f(\omega) \right)^2 \right)}{\left(K_D^2 + \left(\frac{v_m \lambda_i}{\gamma_R \gamma_{P_i}} f(\omega) \right)^2 \right)^3}.
 \end{aligned} \tag{2.30}$$

Although the analytical open-loop results with both opening options are in good agreement with the stochastic simulation algorithm (Figures 2.10 and 2.11), the predicted transition rates, when the feedback is opened from P_1 , deviate from results of stochastic simulation algorithm (Figure 2.12). This confirms the expectation that the loop has to be opened at the slowest variable. If the loop is opened at P_2 , that is, the protein with the slowest decay, the predictions are improved significantly and are in good agreement with the SSA. It is important to note that the predictions for the open-loop variance are equally good. The transitions are generally slower relative to the feedback loop with a single protein (compare Figures 2.12 and 2.8). This is because the four-variable system contains two promoters and the binding to both promoters is cooperative.

2.6 Hidden nonlinearities

In systems with high order reactions, LNA can considerably underestimate the stochastic properties of components [14, 50]. Multiplicative interactions among different components of a system can create a hidden nonlinearity and introduce correlations among noises. These correlations can take positive or negative values depending on whether they are induced by production or degradation processes while the overall effect on the normalized noise is always positive [43]. The strength of such correlations depend on different factors. If components have considerably short half-lives or high concentrations, small correlations might be observed. The drift can be dependent on fluctuations due to the existence of nonlinearities. This dependency is shown mathematically by Stratonovich interpretation [7] and can shift the level of expectation values.

2.7 Calculation of diffusion with correlated white noises

As mentioned before, in a network with different sources of noise, there might be cross-correlated fluctuations which can create complexities in the calculation of the total diffusion. In order to avoid such complexities, we calculate the individual diffusion induced by independent noises from equation (2.20), and then include the cross-correlation effects based on equation (1.8). Consider an arbitrary multidimensional system

$$\begin{aligned} \frac{d}{dt}X_1 &= F_1(X_1) + \sigma_U g_{X_1}(X_1)\xi(t), \\ \frac{d}{dt}X_2 &= F_2(X_1, X_2) + \sigma_U g_{X_2}(X_1, X_2)\zeta(t), \end{aligned} \tag{2.31}$$

where $\xi(t)$ and $\zeta(t)$ are white noises and σ_U is the white noise intensity. Applying the Fokker-Planck equation (2.1) to system (2.31), one gets the following equations which indicate the time evolution of the mean vector X and the covariance matrix C

$$\begin{aligned} \frac{d}{dt}X &= H(X), \\ \frac{d}{dt}C &= J C + (J C)^T + B, \end{aligned} \tag{2.32}$$

where

$$X = \begin{bmatrix} X_1 \\ X_2 \end{bmatrix}, \quad H(X) = \begin{bmatrix} F_1(X_1) \\ F_2(X_1, X_2) \end{bmatrix}, \quad J = \frac{\partial}{\partial X} (H(X)),$$

denote the mean and drift vectors and Jacobian matrix, respectively, and

$$C = \begin{bmatrix} C_{X_1X_1} & C_{X_1X_2} \\ C_{X_1X_2} & C_{X_2X_2} \end{bmatrix}, \quad B = \begin{bmatrix} \sigma_U^2 g_{X_1}^2(X_1) & 0 \\ 0 & \sigma_U^2 g_{X_2}^2(X_1, X_2) \end{bmatrix},$$

represent the covariance and diffusion matrices, respectively. We apply the quasi-steady-state assumption to system (2.31) since X_1 has a fast time-scale compared to X_2 . Therefore, system (2.31) will be reduced to a one-dimensional system in which the effect of different noises are presented individually

$$\frac{d}{dt} \bar{X}_2 = F_2(\bar{X}_2) + \underbrace{\sigma_U g_{X_2}(\bar{X}_2) \zeta(t)}_{\text{Intrinsic Fluctuation}} + \underbrace{\sigma_{X_1} g_{X_1X_2}(\bar{X}_2) X_1(t)}_{\text{Extrinsic Fluctuation}}, \quad (2.33)$$

where $\sigma_{X_1}^2 = C_{X_1X_1}$ and

$$g_{X_1X_2}^2(\bar{X}_2) = \frac{2 \left(\frac{\partial}{\partial X_1} F_2 \right)^2}{\left(\frac{\partial}{\partial X_2} F_2 + \frac{\partial}{\partial X_1} F_1 \right)}, \quad (2.34)$$

is the induced extrinsic diffusion from X_1 to X_2 . For the sake of recognizing the reduced system from the original system, we use \bar{X}_2 and $\bar{C}_{X_2X_2}$ for the reduced system. Nonlinear interactions between the stochastic variables X_1 and X_2 in the second equation in (2.31) indicate that the Stratonovich interpretation should be applied (see Section 1.2.3). System (2.32) can be reduced to the dynamics of X_2 provided that X_1 either has a fast time-scale or is already at the steady state

$$\begin{aligned} \frac{d}{dt} \bar{X}_2 &= H(\bar{X}_2) = F_2(\bar{X}_2) + \frac{1}{4} \frac{d}{d\bar{X}_2} D_{Extrinsic}, \\ \frac{d}{dt} \bar{C}_{X_2X_2} &= 2 \frac{dF_2(\bar{X}_2)}{d\bar{X}_2} \bar{C}_{X_2X_2} + D_{total}. \end{aligned} \quad (2.35)$$

From equation (2.33) with the assumption of having independent noises, the total diffusion D_{total} is given by

$$D_{total} = \underbrace{\sigma_U^2 g_{X_2}^2(\bar{X}_2)}_{D_{Intrinsic}} + \underbrace{\sigma_{X_1}^2 g_{X_1X_2}^2(\bar{X}_2)}_{D_{Extrinsic}}. \quad (2.36)$$

In the reduced system (2.33), $X_1(t)$ and $\zeta(t)$ are the two sources of noise and the cross-correlation between them modifies the total diffusion (2.36) based on

equation (1.8)

$$D_{total} = \underbrace{\sigma_U^2 g_{X_2}^2(\bar{X}_2)}_{D_{Intrinsic}} + \underbrace{\sigma_{X_1}^2 g_{X_1 X_2}^2(\bar{X}_2) + 2\rho_{X_1, \zeta} \sigma_U \sigma_{X_1} g_{X_2}(\bar{X}_2) g_{X_1 X_2}(\bar{X}_2)}_{D_{Extrinsic}},$$

where $\rho_{X_1, \zeta} = \frac{\langle X_1(t), \zeta(t) \rangle}{\sigma_{X_1} \sigma_U}$ is the correlation between $X_1(t)$ and $\zeta(t)$. Since $\rho_{X_1, \zeta}$ cannot be calculated directly, we decompose it into the correlation between two components $\rho_{X_1 X_2}$, multiplied by a normalization factor which reflects the ratio between the variance of X_2 induced by X_1 and the intrinsic variance of X_2 . Therefore, we have

$$D_{total} = \underbrace{\sigma_U^2 g_{X_2}^2(\bar{X}_2)}_{D_{Intrinsic}} + \underbrace{\sigma_{X_1}^2 g_{X_1 X_2}^2(\bar{X}_2) + 2\rho_{X_1 X_2} N_C \sigma_U \sigma_{X_1} g_{X_2}(\bar{X}_2) g_{X_1 X_2}(\bar{X}_2)}_{D_{Extrinsic}}, \quad (2.37)$$

where the correlation between X_1 and X_2 is given using the steady state solution of the covariance matrix C from (2.32)

$$\rho_{X_1 X_2} = \frac{C_{X_1 X_2}}{\sqrt{C_{X_1 X_1} C_{X_2 X_2}}}. \quad (2.38)$$

The normalization factor will be obtained from

$$N_C = \frac{1}{\sqrt{2}} \sqrt{\frac{\frac{\sigma_{X_1 X_2}^2}{\sigma_{X_1}^2}}{\frac{\sigma_{Int X_2}^2}{\sigma_U^2}}}, \quad (2.39)$$

where using equations (2.31) and (2.34), we get

$$\sigma_{X_1 X_2}^2 = -\frac{\sigma_{X_1}^2 g_{X_1 X_2}^2}{2 \frac{\partial}{\partial X_2} F_2}, \quad \sigma_{Int X_2}^2 = -\frac{\sigma_U^2 g_{X_2}^2}{2 \frac{\partial}{\partial X_2} F_2}. \quad (2.40)$$

The former is the induced variance from X_1 to X_2 , and the latter is the intrinsic variance of variables X_2 and X_1 . In fact,

$$C_{X_2 X_2} = \sigma_{X_1 X_2}^2 + \sigma_{Int X_2}^2.$$

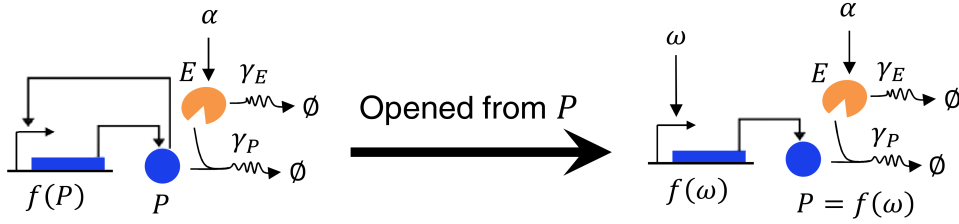


Figure 2.13: A two-component system consisting of an enzyme and a protein. The closed-loop system (left) is opened at the protein level (right).

2.7.1 Example - The effect of multiplicative interactions on MFPT

Multiplicative interactions between components induce correlations between them which can amplify the fluctuations and even shift the mean values. A good example of such phenomena is enzymatic decay in which an enzyme combines with other components to degrade them. With respect to stochastic control, it is particularly interesting to examine how extrinsic components affect the transitions in a feedback loop system. For this purpose, we introduce an enzymatic decay to a protein so that the degradation rate of the protein is multiplied by the concentration of an enzyme and the protein regulates its production within a simple feedback loop. The enzyme displays a Poisson-distribution due to a birth-death process (Figure 2.13)

$$\begin{aligned} \frac{d}{dt}E &= \alpha - \gamma_E E + \sigma_U \sqrt{(\alpha + \gamma_E E)} \xi(t), \\ \frac{d}{dt}P &= f(P) - \gamma_P EP + \sigma_U \sqrt{f(P) + \gamma_P EP} \zeta(t), \end{aligned} \quad (2.41)$$

where $\xi(t)$ and $\zeta(t)$ are white noises, $\sigma_U = 1$ (for simplicity) is the white noise intensity and

$$f(P) = b + v_m \frac{P^2}{K_D^2 + P^2}. \quad (2.42)$$

If we open the feedback loop at the level of protein, with the mean vector and the covariance matrix

$$X = \begin{bmatrix} E \\ P \end{bmatrix}, \quad C = \begin{bmatrix} C_{EE} & C_{EP} \\ C_{EP} & C_{PP} \end{bmatrix},$$

the reaction rates vector and the stoichiometry matrix will be

$$V = \begin{bmatrix} \alpha & \gamma_E E & f(\omega) & \gamma_P EP \end{bmatrix}^T, \quad S = \begin{bmatrix} 1 & -1 & 0 & 0 \\ 0 & 0 & 1 & -1 \end{bmatrix},$$

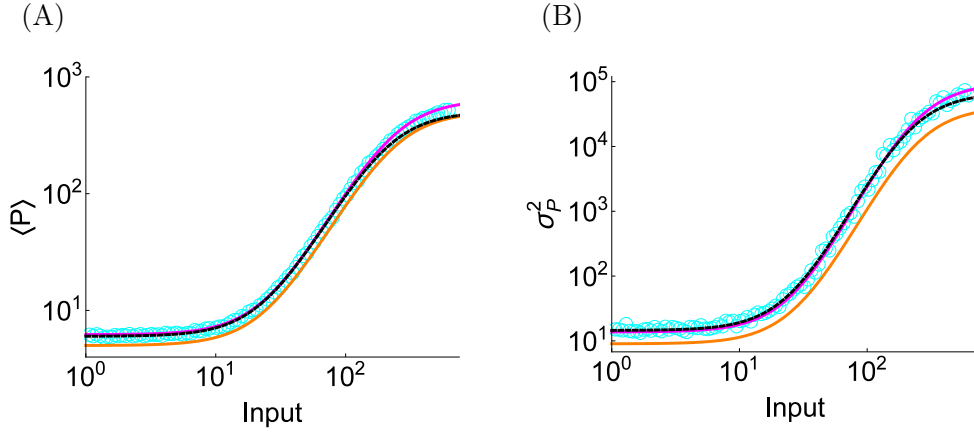


Figure 2.14: A two-component system consisting of an enzyme and a protein. (A) The open-loop response and (B) the variance of the output with respect to the input are calculated by the stochastic simulation algorithm (cyan circle) and the analytical approach when the fluctuations are uncorrelated (orange solid) or cross-correlated (magenta solid). For uncorrelated fluctuations, the Ito method is used whereas the Stratonovich interpretation is used for cross-correlated noises. The protein is degraded by an enzyme, which displays a Poisson distribution due to a birth-death process, with $\alpha = 1.25$, $\gamma_E = 0.25$. The black dashed curves are functions fitted to the mean and variance of P_2 (see 2.8.1). The following parameters are fixed: $K_d = 110$, $v_m = 500$, $b = \frac{v_m}{100}$, $\gamma_P = 0.2$ and $n = 2$.

and

$$J = \begin{bmatrix} -\gamma_E & 0 \\ -\gamma_P P & -\gamma_P E \end{bmatrix}, \quad B = \begin{bmatrix} \alpha + \gamma_E E & 0 \\ 0 & f(\omega) + \gamma_P EP \end{bmatrix},$$

denote the Jacobian and diffusion matrices, respectively. Therefore, the time evolution of the corresponding mean vector X and covariance matrix C for system (2.41) will be obtained from (1.10) which can be reduced to the following system provided that the enzyme is at the steady state (see equation (2.35))

$$\begin{aligned} \frac{d}{dt} \bar{P} &= f(\omega) - \gamma_P E_s \bar{P} = H_I(P), \\ \frac{d}{dt} \bar{C}_{PP} &= -2\gamma_P E_s \bar{C}_{PP} + D_{total}, \end{aligned} \tag{2.43}$$

where using equation (2.20), the total diffusion induced by independent white noises will be

$$D_{total} = \underbrace{f(\omega) + \gamma_P E_s \bar{P}}_{D_{Intrinsic}} + \underbrace{\frac{2(\gamma_P \bar{P})^2 E_s}{(\gamma_E + \gamma_P E_s)}}_{D_{Extrinsic}}. \tag{2.44}$$

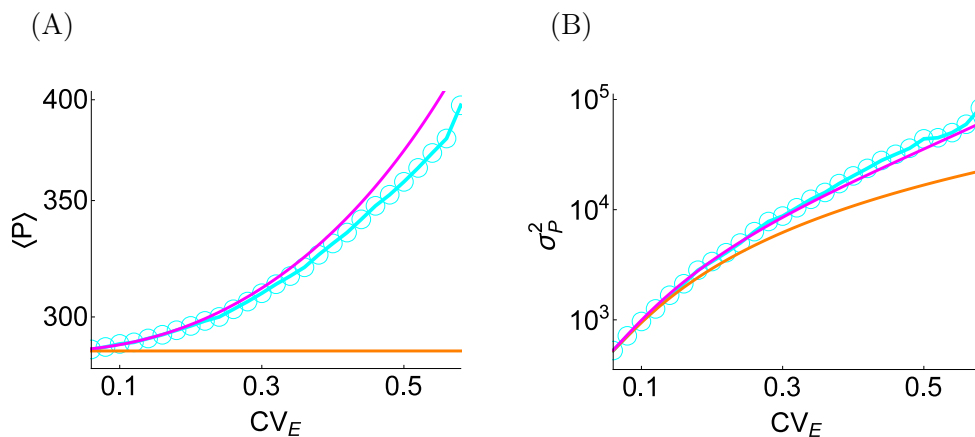


Figure 2.15: The same model as in Figure 2.14 is studied with the following differences. The production rate of the enzyme is tuned to $\alpha = \frac{0.25}{CV_E^2}$ to adjust the coefficient of the enzyme variation level at the steady-state CV_E . To keep the decay of protein constant, the decay rate constant γ_P is varied to compensate the variations in the enzyme concentration: $\gamma_P = CV_E^2$. (A) The open-loop response and (B) the variance of the output with respect to CV_E are shown for Input = 125, $K_D = 130$. The stochastic simulation algorithm results (cyan circle) match with that of the analytical approach with correlated noises (solid magenta). The total diffusion is shown for the correlated noise (solid black).

For the sake of recognizing the reduced system from the original system, we use \bar{P} and \bar{C}_{PP} for the reduced system. With the drift and diffusion from (2.43) and (2.44), the calculated MFPT values from (2.11) are deviated considerably from the ones obtained from the stochastic simulation algorithm (orange and cyan curves in Figures 2.16–2.18). Furthermore, the value of the open-loop output is deviated slightly but consistently from the values obtained from the stochastic simulation algorithm (orange and cyan curves in Figures 2.14 and 2.15). This is not surprising because it has been known that in the presence of high-order reactions, the LNA is not accurate anymore. Nonlinear interactions in (2.41) will introduce a cross-correlation effect to the total diffusion (2.44). Therefore, from equation (2.37), the total diffusion containing the cross-correlation effect will be modified as follows

$$\begin{aligned}
 D_{total} = & \underbrace{f(\omega) + \gamma_P E_s \bar{P}}_{D_{Intrinsic}} \\
 & + \underbrace{\frac{2(\gamma_P \bar{P})^2 E_s}{(\gamma_E + \gamma_P E_s)} - 2\rho_{EP} N_C \gamma_P \bar{P} \sqrt{\frac{2E_s}{(\gamma_E + \gamma_P E_s)} (f(\omega) + \gamma_P E_s \bar{P})}}_{D_{Extrinsic}}, \quad (2.45)
 \end{aligned}$$

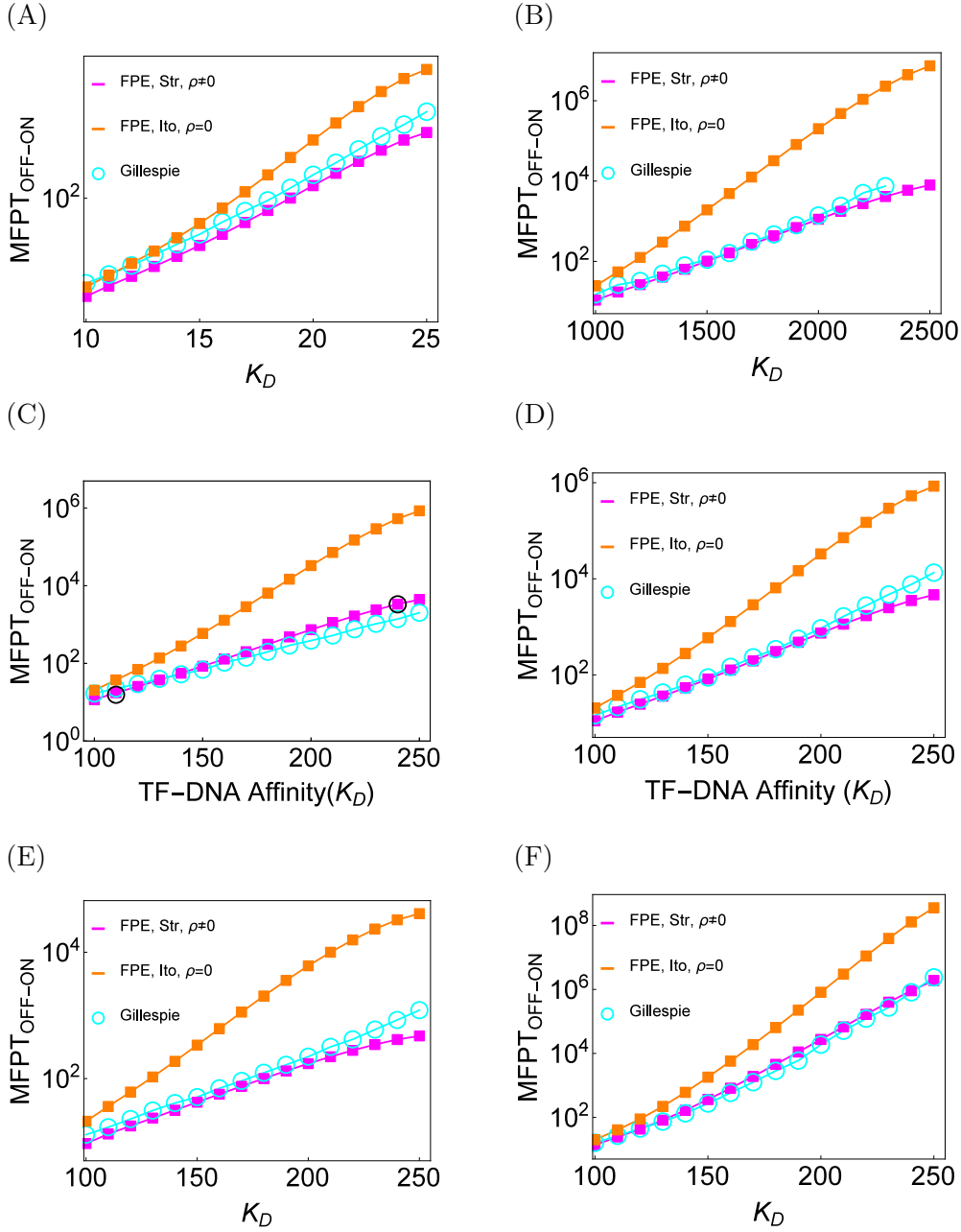


Figure 2.16: The MFPT from OFF to ON state for system (2.41) is calculated for the bistable range of the K_D with the following fixed parameter values: $b = \frac{v_m}{100}, \gamma_P = \frac{1}{E_s}$, (A) $v_m = 50, \gamma_E = 0.5, E_s = 5$, (B) $v_m = 5000, \gamma_E = 0.5, E_s = 5$, (C) $v_m = 500, \gamma_E = 0.25, E_s = 5$, (D) $v_m = 500, \gamma_E = 0.5, E_s = 5$, (E) $v_m = 500, \gamma_E = 0.5, E_s = 3$, (F) $v_m = 500, \gamma_E = 0.5, E_s = 10$. The black circles represent the MFPT which is calculated using the drift and diffusion fitted to open-loop data.

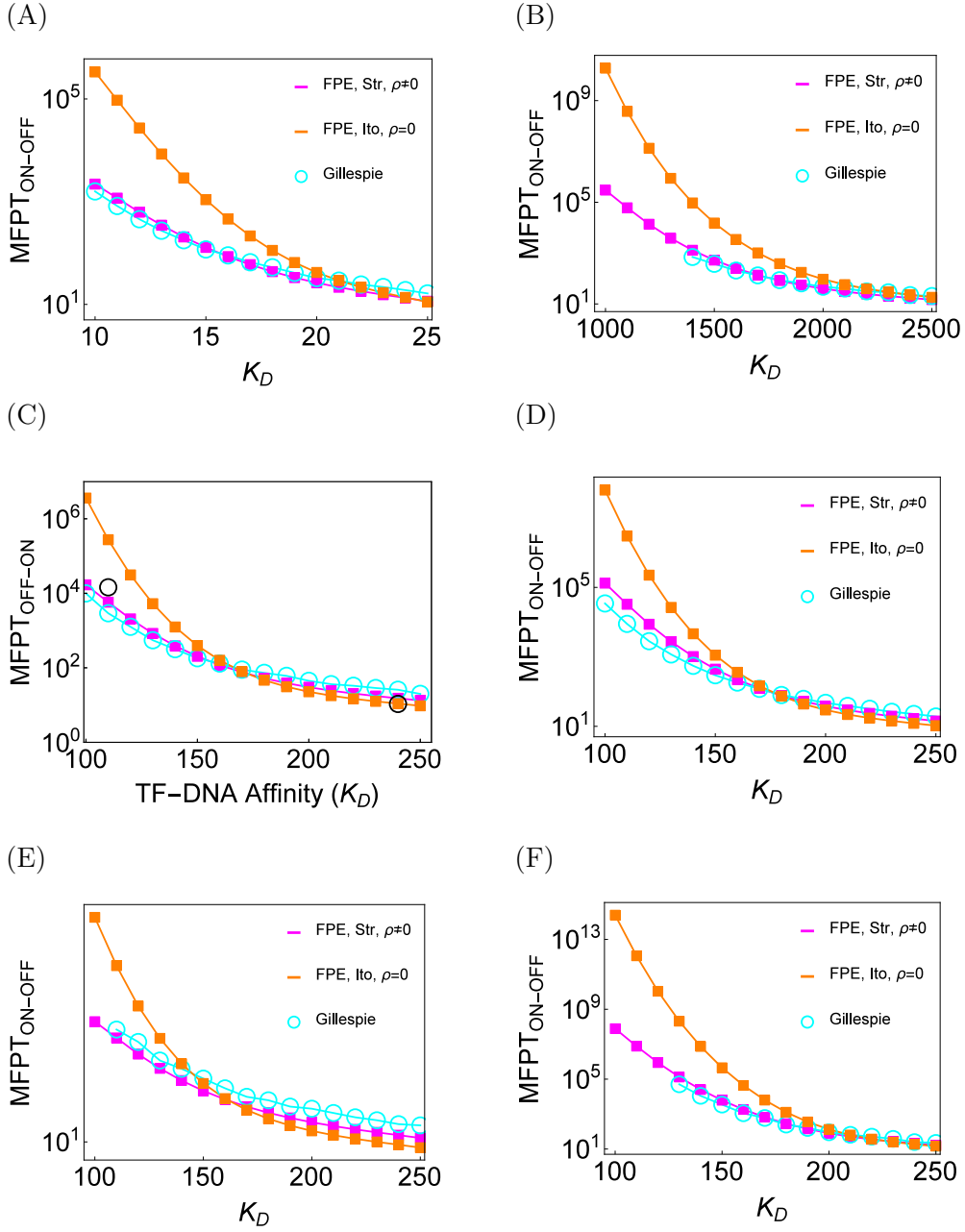


Figure 2.17: The MFPT from ON to OFF state for system (2.41) is calculated for the bistable range of the K_D with the following fixed parameter values: $b = \frac{v_m}{100}$, $\gamma_P = \frac{1}{E_s}$, (A) $v_m = 50$, $\gamma_E = 0.5$, $E_s = 5$, (B) $v_m = 5000$, $\gamma_E = 0.5$, $E_s = 5$, (C) $v_m = 500$, $\gamma_E = 0.25$, $E_s = 5$, (D) $v_m = 500$, $\gamma_E = 0.5$, $E_s = 5$, (E) $v_m = 500$, $\gamma_E = 0.5$, $E_s = 3$, (F) $v_m = 500$, $\gamma_E = 0.5$, $E_s = 10$. The black circles represent the MFPT which is calculated using the drift and diffusion fitted to open-loop data.

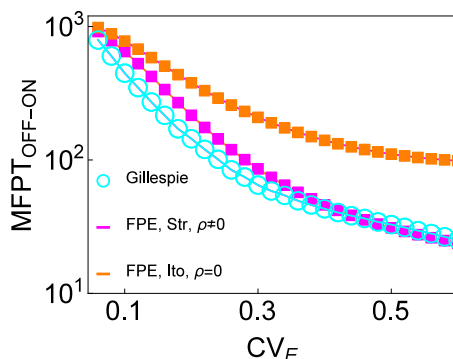


Figure 2.18: The closed-loop result of the model was studied in Figure 2.15. The MFPT for protein from the OFF to ON state is shown as CV_E was varied. The good agreement between the results of the stochastic simulation algorithm (cyan circle) and the analytical approach (magenta rectangle) reflects the importance of the correlation between noises. The parameters are fixed at $v_m = 500$, $b = \frac{v_m}{100}$, $\gamma_P = CV_E^2$, $\gamma_E = 0.25$, $\alpha = \frac{1}{4}CV_E^2$, $K_D = 130$.

where E_s represents the steady-state concentration of enzyme and

$$\rho_{EP} = \frac{C_{EP}}{\sqrt{C_{EE}C_{PP}}} = \frac{-\frac{\gamma_P E_s \bar{P}}{(\gamma_P E_s + \gamma_E)}}{\sqrt{\frac{1}{\gamma_P} \left(\frac{(\gamma_P \bar{P})^2 E_s}{(\gamma_P E_s + \gamma_E)} + (f(\omega)) \right)}}$$

Having σ_{EP}^2 and $\sigma_{P,Int}^2$ based on equations (2.40), the normalization factor N_C is calculated from (2.39)

$$N_C = \frac{1}{\sqrt{2}} \sqrt{\frac{\frac{\sigma_{EP}^2}{\sigma_E^2}}{\frac{\sigma_{IntP}^2}{\sigma_U^2}}} = \sqrt{\frac{(\gamma_P \bar{P})^2}{2(\gamma_P E + \gamma_E)(f(\omega))}}.$$

The nonlinear interactions between protein and enzyme correlate the deterministic and stochastic part of the system obtained by Stratonovich interpretation

$$\begin{aligned} H_S(\omega, \bar{P}) &= H_I(\omega, \bar{P}) + \frac{1}{4} \frac{d}{d\bar{P}} D_{Extrinsic} \\ &= f(\omega) - \gamma_P E_s \bar{P} + \frac{1}{4} \frac{d}{d\bar{P}} D_{Extrinsic}. \end{aligned} \quad (2.46)$$

The drift in the Ito interpretation, H_I , corresponds simply to the dynamics of the deterministic system. The drift in the Stratonovich interpretation is extended by adding the derivative of the external diffusion with respect to the system variable \bar{P} to H_I . Figures 2.14 and 2.15 (magenta curve) show that

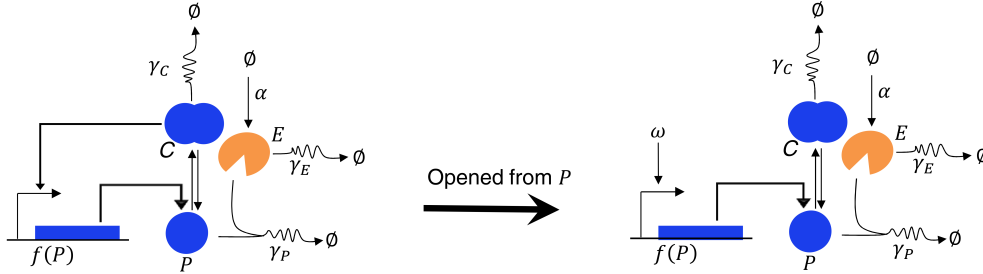


Figure 2.19: A three-component system consisting of an enzyme, a protein and a protein dimerization. The closed-loop system (left) is opened at the protein (right).

the introduction of cross-correlated noises decrease the discrepancy between the stochastic simulation algorithm and the theoretical results in the open-loop system. With the drift and diffusion from (2.44) and (2.45), after closing the loop, we can calculate the MFPT from equation (2.11) with the boundary condition (2.12) for different parameter values. The mean first passage time from low to high and from high to low protein concentrations is calculated for the range of bistability with respect to K_D . The satisfactory agreement between the results of the stochastic simulation algorithm (cyan circle) and the analytical approach (magenta rectangle) implies the importance of the cross-correlation between noises (Figures 2.16–2.18).

2.7.2 Example - The effect of different nonlinearities on MFPT

In order to validate our analytical method with different nonlinearities, we replace the simple positive feedback loop in the previous example with a protein dimerization and cooperative binding (Figure 2.19). Therefore,

$$f(\omega) = V_m \frac{\omega_{id}^{n_1} d\omega^{n_2}}{k_1 + \omega_{id}^{n_1} d\omega^{n_2}} + b, \quad (2.47)$$

where

$$\omega_{id} = \omega + \frac{\kappa - \sqrt{4\omega\kappa + \kappa^2}}{2}.$$

With the drift and the total diffusion obtained from equations (2.45) and (2.46) and the input function (2.47), we can calculate the mean first passage time using equation (2.11) with the boundary condition (2.12). The satisfactory agreement between the stochastic simulation algorithm and the analytical approach indicates the validity of our approach for systems with different nonlinearities (Figure 2.20).

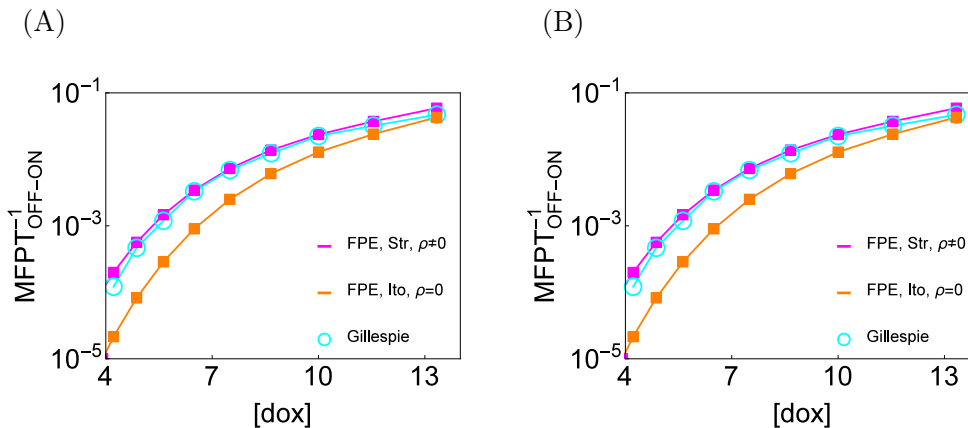


Figure 2.20: The MFPT for protein from OFF to ON state is shown for (A) $E_s = 10$ and (B) $E_s = 20$. The good agreement between the results of the stochastic simulation algorithm (cyan circle) and the analytical approach (magenta rectangle), and the discrepancy with the results obtained from uncorrelated noises (orange rectangle) indicate the importance of the correlation between noises.

2.8 Experimental applications of the open-loop approach

The above results indicate that the drift and diffusion of the open-loop output faithfully reflect the stochastic system dynamics and can be used to calculate the MFPT even when the expectation value of the output is shifted by noise. The question remains as to how the above findings can be used to predict the MFPT from experimental measurements in which neither the drift nor the diffusion can be measured analytically.

The open-loop function can be used to identify the steady-state expression of the output and consequently map the steady-state expression levels for the closed-loop system [1]. The open-loop function reflects only the relationship between the input and output and lacks information on the time scale of the reactions and key parameters, which are required to predict the transition rates. The above analytical approach can help us determine proper functions to fit to the data obtained from the open-loop systems. Those functions can be later used in the closed-loop system to calculate the MFPT. In order to model the drift and diffusion which are necessary elements in the MFPT calculation, we need to incorporate all possible sources of noise into the function that we use to fit the mean and variance of the output. The open-loop function can be used to distinguish the underlying molecular mechanism. Preliminary knowledge of the

kinetic reactions involved in the system lead us to design a construct and write the corresponding equations for mean values and co/variances. The validity of the model can be examined using the stochastic simulation algorithm for both mean values and the variances. We come up with alternative modifications in the later stages of our analysis.

For the time dependent behaviors, the open-loop function has to be extended into a model, which incorporates information on the time-scale of the reactions as well. The following relations provide the link between the drift and diffusion and fitted functions to the mean ($f(\omega)$) and variance ($C_p(\omega)$) of the output using experimental measurements. The diffusion and variance are linked by the decay rate of the output γ_p

$$D_{total}(\omega) = -2\gamma_p C_p(\omega, \eta), \quad (2.48)$$

and the drift can be obtained directly from

$$H(\omega) = \gamma_p (f(\omega) - \eta). \quad (2.49)$$

Upon reclosing the loop, $\omega = \eta$, we obtain the functions for the drift and diffusion in the closed-loop system, and therefore, the MFPT can be predicted. The chosen functions to be fitted to the open-loop data can create a considerable discrepancy between MFPT predicted by theoretical approach and that obtained from experimental data.

2.8.1 Example - A two-component system consisting of an enzyme and a protein

Consider the two-dimensional closed-loop system (2.41) in which the enzyme is an external source of fluctuation for the protein. By opening the feedback loop at the protein level and considering the quasi-steady state assumption for enzyme, the time evolution of the corresponding mean values and co/variances can be reduced to a one-dimensional system with the drift and total diffusion obtained from (2.46) and (2.29), respectively. Nonlinear regression is used to fit the parameters of the open-loop function $f(\omega)$ obtained from (2.42) to the open-loop results of the stochastic simulation algorithm. The corresponding function to fit the variance C_p in an open-loop system, which is obtained from equation (2.45), contains both input and output as variables. Since the open-loop results are calculated at the steady state, the output can be replaced by its equivalent value which is the fitted open-loop function. Therefore, we use the fitted open-

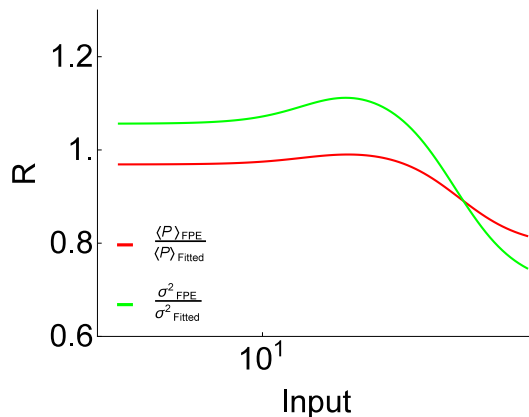


Figure 2.21: The ratio (R) between the steady states mean (red) and variance (green) of the open-loop system (2.43) obtained from the FPE, and those obtained by fitting the parameters to the open-loop results of stochastic simulation algorithm with respect to input. The closer the value of R to one is, the closer the two methods predictions will be.

loop function as a constant to fit the parameters in the corresponding variance function. Thus,

$$C_P = \frac{D_{total}}{2\gamma_P} = \frac{f(\omega) + \gamma_P E_s P}{2\gamma_P} + \frac{\gamma_P E_s P^2}{(\gamma_E + \gamma_P E_s)} \Big|_{P=f(\omega)}.$$

Figure 2.21 shows the ratio between the stochastic properties of the open-loop system (2.43) obtained from the FPE and those obtained by fitting the parameters to the open-loop results of the stochastic simulation algorithm. It should be noted that the type of nonlinearity in the mentioned fitted functions plays a crucial role in the MFPT calculation in the closed-loop system. After reclosing the loop, those terms in which the output is replaced by a fitted open-loop function should be again replaced by the output. The total diffusion and the drift can be obtained using the mentioned fitted functions based on equations (2.48) and (2.49). With the drift and diffusion, we can use equation (2.11) with the boundary conditions (2.12) to calculate the MFPT. Figure 2.16(C) and 2.17(C) show an agreement between the MFPT calculated by using the fitted drift and diffusion (2.49) and (2.48) (black circles), and that predicted by the stochastic simulation algorithm (cyan circle).

2.8.2 Example - A four-component system consisting of two RNAs and two proteins

Consider the four-dimensional closed-loop system (2.25) with the assumption of P_2 having the slowest time scale. Therefore, by opening the feedback loop

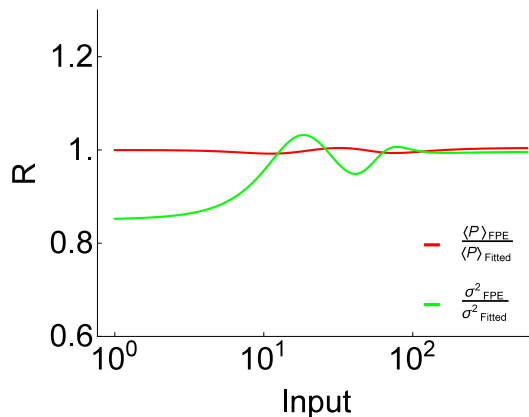


Figure 2.22: The ratio (R) between the steady states mean (red) and variance (green) of the open-loop system (2.28) obtained from the FPE, and those obtained by fitting the parameters to the open-loop results of stochastic simulation algorithm with respect to the input. The closer the value of R to one is, the closer the two methods predictions will be.

at P_2 and considering the quasi-steady state assumption for RNAs and P_1 , the time evolution of the corresponding mean values and co/variances will be reduced to the one-dimensional system (2.28) with the drift and total diffusion obtained from (2.30) and (2.29), respectively. Nonlinear regression is applied to fit the parameters of the open-loop function $f(\omega)$ and the output variance C_p to the open-loop results of stochastic simulation algorithm. The open-loop function $f(\omega)$ is defined in equation (2.26) and the output variance C_p can be obtained using (2.48) and (2.29), respectively. Figure 2.22 shows the ratio between the stochastic properties of the open-loop of the mentioned system obtained from the FPE and those obtained by fitting the parameters to the open-loop results of the stochastic simulation algorithm. The total diffusion and the drift can be obtained using the mentioned fitted functions based on equations (2.48) and (2.49). With the drift and diffusion, we can use equation (2.11) with the boundary conditions (2.12) to calculate the MFPT. Figure 2.16 shows an agreement between the MFPT, calculated by using the fitted drift and diffusion (2.48) and (2.49) (black circles), and that obtained from the stochastic simulation algorithm (cyan circle).

2.8.3 Example - The effect of homodimerization and cooperativity on transition rate

Consider a feedback loop incorporating cooperative binding with protein dimerization which introduce nonlinearities into the system. The effects of such nonlinearities on cellular memory are investigated through the transition rates ob-

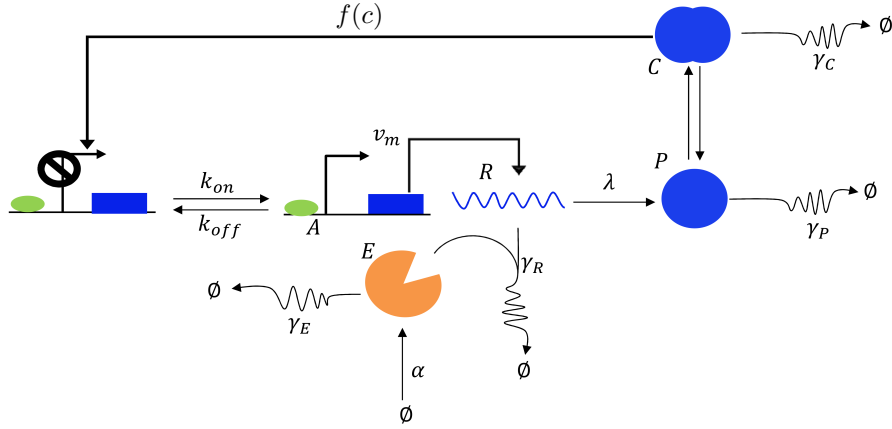


Figure 2.23: A feedback loop system incorporating protein dimerization and cooperative binding. The RNA has an enzymatic decay and regulates the level of protein. Active promoter (A) regulates the level of RNA. The enzyme (E) and the protein (monomer P and dimer C) have a linear decay.

tained for the slowest variable. Noise induced transitions between the two states of a system require that both states become populated which results in a bimodal distribution. The interplay between noise and the slow transient induction may create a broader bimodality area than the bistability area in the parameter space. Feedback opening can help identify the molecular mechanisms that are responsible for such an expansion. In the mentioned system, nonlinear regression is used to fit the open-loop function $f(\omega)$ to the data obtained from the open-loop systems. To reconstruct the feedback loops, the open-loop system is re-closed by setting the input ω equal to the output RNA. The validity of the obtained closed-loop system is approved by having a good agreement between the closed-loop steady-state obtained from the analytical approach and that predicted by experimental data. The experimental data in this example are provided by Hsu et al. [18]. Preliminary design of the construct suggests to have the Hill function for cooperative binding to promoter along with the protein dimerization process. Alternative modifications are introduced in the later stages (Figure 2.23). The function fitted to the experimental open-loop data of the monomeric cooperative binding to the promoter $P_{[tetO]_{7sc}}$ is given by

$$f(\omega) = V_m \frac{\omega^{n_1} d\omega^{n_2}}{k_1 + \omega^{n_1} d\omega^{n_2}} + b, \quad (2.50)$$

while for the dimeric cooperative binding to the promoter $P_{[tetO]_7}$, the fitted function is

$$f(\omega) = V_m \frac{\omega_{id}^{n_1} d\omega^{n_2}}{k_1 + \omega_{id}^{n_1} d\omega^{n_2}} + b, \quad (2.51)$$

where

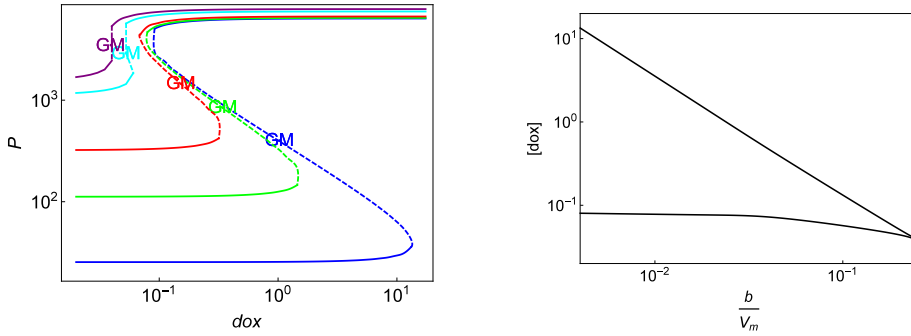


Figure 2.24: The feedback loop is composed of a dimeric protein and the promoter $P_{[tetO]_7}$. (A) The hysteresis curves are depicted for b/V_m equals 0.004 (blue), 0.0176 (green), 0.051 (red), 0.177 (cyan) and 0.243 (purple). (B) Bistability range varies by modulating basal expression level. The geometric mean of stable steady states, labeled with GM, is calculated at the dox value of the geometric mean of the bistability boundaries.

$$\omega_{id} = \omega + \frac{\kappa - \sqrt{4\omega\kappa + \kappa^2}}{2}. \quad (2.52)$$

The introduced fitting function contains the following lumped parameter

$$\kappa = \frac{\delta_{mo}^2(K_d + \delta_{di})}{4\delta_{di}^2 k_a}, \quad (2.53)$$

where δ_{mo} , δ_{di} , k_a and K_d are the monomer and dimer decay rate constants, and association and dissociation rate constants in the dimerization process, respectively [5]. Figures 2.24 and 2.25 correspond to the hysteresis and the bistability area with respect to the concentration of doxycycline $[dox]$ and the dynamic range of the open-loop response b/V_m .

So far the introduced open- and closed-loop systems have been considered at the steady state. In the analysis of time dependent behaviors, the information on the time-scale of the reactions should be taken into account. Considering the time scale of the RNA and γ_R and using equation (2.49), one can get the time evolution of the output RNA as follows

$$\frac{d}{dt}R = \gamma_R(f(\omega) - R), \quad (2.54)$$

where R represents the concentration of RNA. The corresponding closed-loop system is given by

$$\frac{d}{dt}R = \gamma_R(f(R) - R). \quad (2.55)$$

In order to check the validity of the introduced model, the results of the analyt-

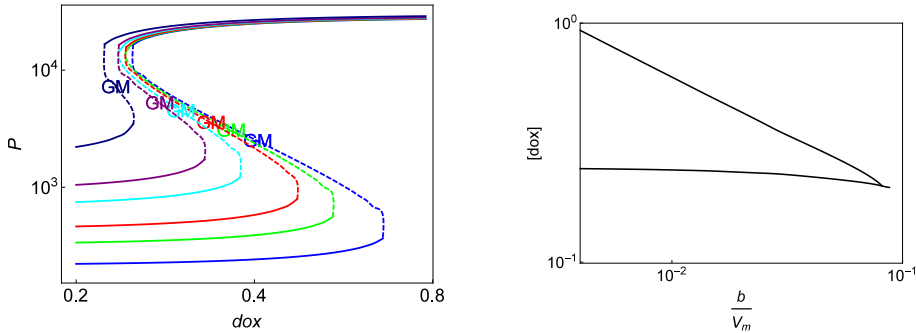


Figure 2.25: The feedback loop is composed of a monomeric protein and the promoter $P_{[tetO]_{\gamma_{sc}}}$. (A) The hysteresis curves are depicted for b/V_m equals 0.0077 (blue), 0.0116 (green), 0.0156 (red), 0.0245 (cyan), 0.033 (purple) and 0.061 (dark blue). (B) Bistability range varies by modulating basal expression level. The geometric mean of stable steady states, labeled with GM, is calculated at the dox value of the geometric mean of the bistability boundaries.

ical approach are compared to the ones obtained from the stochastic simulation algorithm. The detection of transition rates are preceded by a pre-run for a time period of the protein half-life to obtain the probability distribution for a given initial condition. In order to include the fluctuations, the one-dimensional system is extended to include other stochastic components. In the simplest multivariable system, the protein dynamics are added to equations (2.54) and (2.55). Thus, the reactions for the RNA and protein turnover are specified in the following open-loop system

$$\begin{aligned} \frac{d}{dt}R &= \gamma_R(f(\omega(P)) - R), \\ \frac{d}{dt}P &= \rho\omega - \gamma_PP, \end{aligned} \quad (2.56)$$

where $\omega(P) = \frac{\gamma_PP}{\rho}$. The corresponding co/variance equations are obtained based on equation (2.1) with the diffusion matrix

$$B = \begin{bmatrix} 2\gamma_R R & 0 \\ 0 & 2\gamma_PP \end{bmatrix}. \quad (2.57)$$

The closed-loop system can be reconstructed by putting $\omega = R$ in equation (2.56). Although the open-loop data confirm the validity of the introduced model, the transition rates predictions by closed-loop system (2.56) are overestimated compared to the experimental results. This shows that the closed-loop system needs to contain more fluctuations. In the next step, system (2.56) is extended to incorporate two active promoters A_b and A_f which produce RNA, and an enzyme

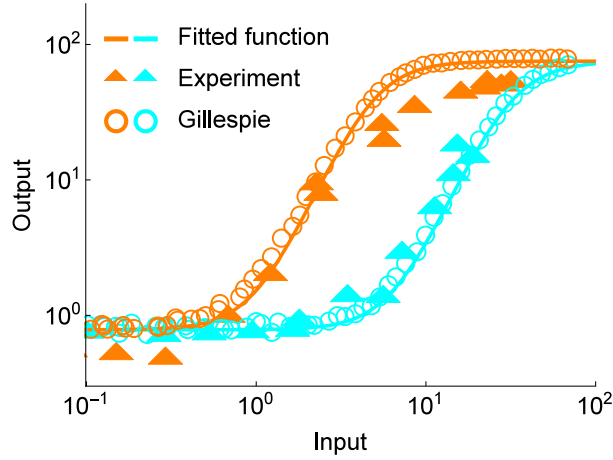


Figure 2.26: Mean values of the output in the system with dimeric binding to the promoter $P_{[TetO]_7}$. Comparison between the results of experimental data (triangles), fitted model (solid line) and the stochastic simulation algorithm (circles) of system (2.58). The results are depicted for the dox values of 0.06 (cyan) and 3.6 (orange).

E which degrades RNA

$$\begin{aligned}
 \frac{d}{dt}A_b &= \lambda_{on_b}(1 - A_b) - \lambda_{off}A_b, \\
 \frac{d}{dt}A_f &= \lambda_{on_f}(1 - A_f) - \lambda_{off}A_f, \\
 \frac{d}{dt}E &= \alpha - \gamma_E E, \\
 \frac{d}{dt}R &= V_m(A_f + A_b) - \gamma_R \frac{E}{E_s} R, \\
 \frac{d}{dt}P &= \rho\omega - \gamma_P P.
 \end{aligned} \tag{2.58}$$

The promoter activation rates λ_{on_b} and λ_{on_f} are defined as follows

$$\lambda_{on_b} = \frac{\lambda_{off}b}{V_m - b}, \quad \lambda_{on_f} = \frac{\lambda_{off}f(\frac{\gamma_P P}{\rho})}{V_m - f(\frac{\gamma_P P}{\rho})}. \tag{2.59}$$

In order to set the same burst size for the promoters, the same inactivation rates λ_{off} are taken for both promoters. The time evolution of the covariance matrix corresponding to system (2.58) is given by

$$\dot{C} = JC + CJ^T + B, \tag{2.60}$$

in which J is the Jacobian matrix of system (2.58), and

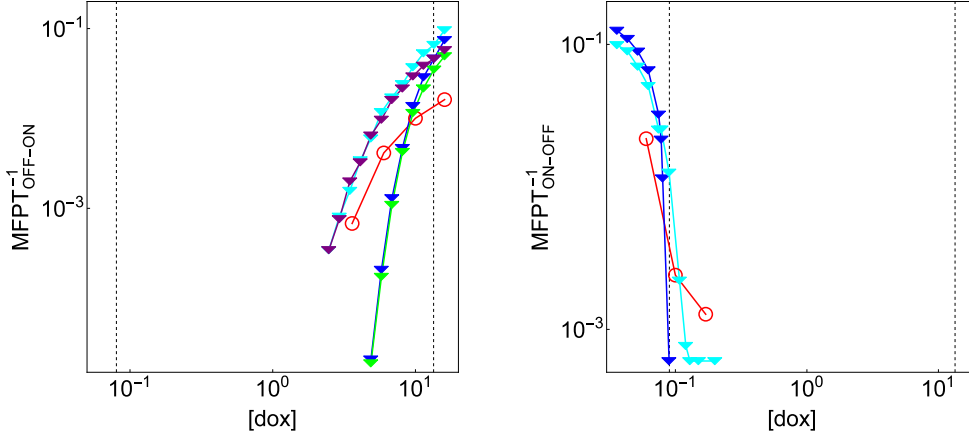


Figure 2.27: The measured and predicted transition rates for the dimeric binding to the promoter $P_{[tetO]_7}$. The dashed gray lines correspond to the bistability boundaries. The red circles represent the experimentally measured transition rates. The green and blue triangles denote the transition rates for the 2D-model (2.56) in the closed-loop setting with and without transient kinetic, respectively. The purple and cyan curves indicate the transition rates after closing system (2.58) with and without transient kinetic, respectively. (A) Transition rates from low to high concentrations. (B) Transition rates from high to low concentrations. The parameters are fixed at $\rho = 0.54$, $abs = 2.11$, $id = 1.407$, $\mu = 0.2291$, $\delta = 0.0095$, $V_1 = 74.4773$, $n_1 = 1.46191$, $n_2 = 1.32$, $k_1 = 0.0356466$, $\kappa = 719.655$, $V_m = \mu V_1 abs/id$, $k_{off} = 13.33$, $E_s = 21$, $d_i = \ln(2)/120$, $k_i = 1$, $n_i = 0.751286$.

$$C = \begin{bmatrix} C_{A_b A_b} & C_{A_b A_f} & C_{A_b E} & C_{A_b R} & C_{A_b P} \\ C_{A_b A_f} & C_{A_f A_f} & C_{A_f E} & C_{A_f R} & C_{A_f P} \\ C_{A_b E} & C_{A_f E} & C_{EE} & C_{ER} & C_{EP} \\ C_{A_b R} & C_{A_f R} & C_{ER} & C_{RR} & C_{RP} \\ C_{A_b P} & C_{A_f P} & C_{EP} & C_{RP} & C_{PP} \end{bmatrix}, \quad (2.61)$$

is the covariance matrix. Additionally

$$B = \begin{bmatrix} 2\lambda_{off} A_b & 0 & 0 & 0 & 0 \\ 0 & 2\lambda_{off} A_f & 0 & 0 & 0 \\ 0 & 0 & 2\gamma_E E & 0 & 0 \\ 0 & 0 & 0 & 2\gamma_R R & 0 \\ 0 & 0 & 0 & 0 & 2\gamma_P P \end{bmatrix}, \quad (2.62)$$

is the diffusion matrix. In the extended system (2.58), the closed-loop system can be reconstructed by taking $\omega = RNA$. All the parameters of system (2.58) are obtained from experimental data, except the inactivation rate of promoters λ_{off} and the enzyme steady state level E_s . These two parameters are calcu-

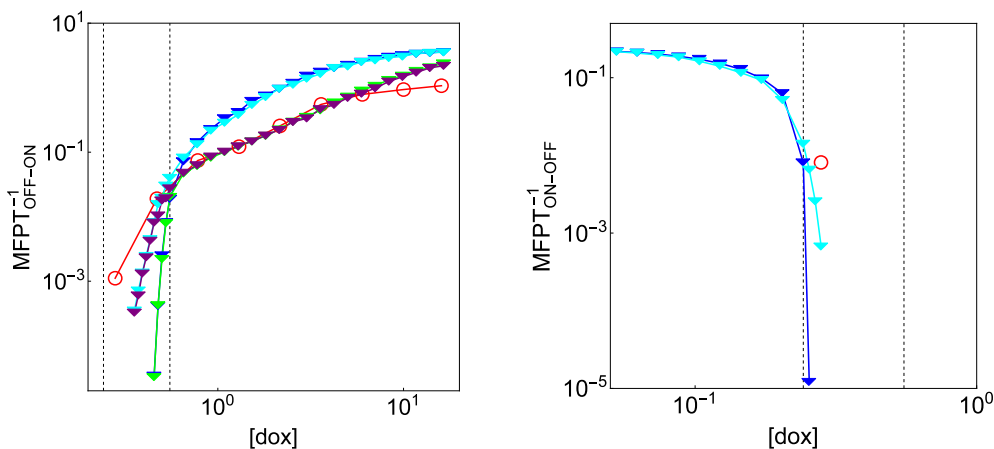


Figure 2.28: The measured and predicted transition rates for the monomeric binding to the promoter $P_{[tetO]_7}$. The dashed gray lines correspond to the bistability boundaries. The red circles represent the experimentally measured transition rates. The green and blue triangles denote the transition rates for 2D-model (2.56) in the closed-loop setting with and without transient kinetic, respectively. The purple and cyan curves indicate the transition rates after closing system (2.58) with and without transient kinetic, respectively. (A) Transition rates from low to high concentrations. (B) Transition rates from high to low concentrations. The parameters are fixed at $\rho = 4.836$, $abs = 2.31$, $id = 2.295$, $\mu = 0.2291$, $\delta = 0.0095$, $V_1 = 54.6379$, $n_1 = 1.94223$, $n_2 = 1.9$, $k_1 = 8.70762$, $V_m = \mu V_1 abs/id$, $k_{off} = 11.52435120$, $E_s = 21$, $d_i = \ln(2)/120$, $k_i = 1$, $n_i = 0.751286$.

lated in a way that the normalized noise of the closed-loop system predicted by the analytical approach has the same values as it is predicted by the experimental data. Although the extended system (2.58) predicts the experimental data from the open-loop systems accurately, there is still a considerable discrepancy between transition rates measured by experimental data and the stochastic simulation algorithm. In order to track this problem, the time evolution of the output is being analyzed. Interestingly, the induction of expression is slower than the half-life of the protein and RNA. The slow induction can arise due to the slow transient kinetics in the open-loop system and slow down the transition rates in the closed-loop system. In order to introduce such modifications, an Ornstein-Uhlenbeck process $i(t)$ with the decay rate of d_i is included in the open-loop system which modifies the parameter k_1 in the fitted functions (2.50) and (2.51)

$$k_{1_{new}} = k_1(1 + k_i i(t))^{n_i},$$

where parameter n_i , k_i and d_i are calculated by fitting the new output to the experimental data. A system can experience unexpected frequent transitions when the steady states are close to each other. Therefore, separation of the

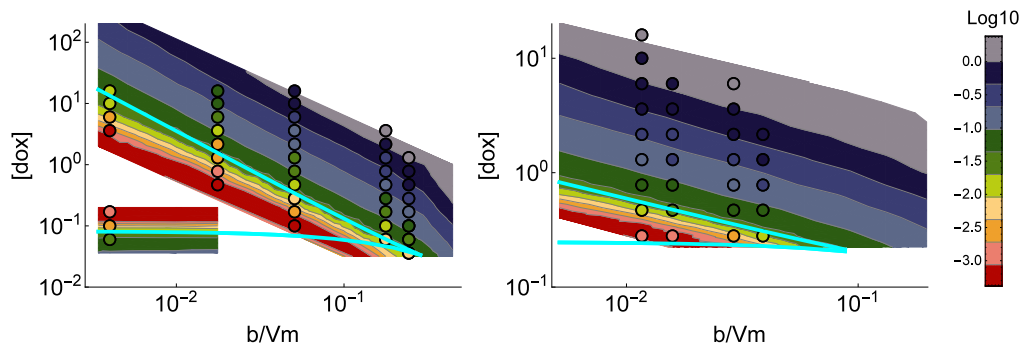


Figure 2.29: Transition rates predicted by the stochastic simulation algorithm (contour diagram) and obtained from the experimental data (circles) in a two-dimensional parameter space. Parameter values for the observed transition rates are given in Figures 2.27 and 2.28. The difference between the transition rates predicted by the stochastic simulation algorithm and experimental data can be seen by the distance in the color-scale. (A) Transition rates from OFF to ON in the system with dimeric binding to the promoter $P_{[tetO]_7}$. The inset in the bottom left corner depicts the transitions from ON to OFF steady state. (B) Transition rates from OFF to ON in the system with monomeric binding to the promoter $P_{[tetO]_{7sc}}$.

peaks of the probability distribution can be taken as a robustness measure of cellular memory. It is important to investigate the conditions under which the two peaks of a distribution merge and the distribution becomes unimodal. The extrema of the probability distribution can be obtained using

$$\begin{aligned}
 H(P) &= \rho f\left(\frac{\gamma_P P}{\rho}\right) - \gamma_P P - \frac{1}{4} \frac{d}{dP} D(P) = 0, \\
 \frac{d}{dP} H(P) &= 0,
 \end{aligned}
 \tag{2.63}$$

where $D(P)$ is the diffusion. The range of bimodality predicted by (2.63) is relatively broader than the bistability range and can be explained by a high level of fluctuations in the extended system (2.58). In order to calculate the transition rates, we perform the stochastic simulation algorithm for the extended system (2.58) in the closed-loop setting. In order to obtain the distribution for the given initial condition, a pre-run for the time period of the protein half-life is performed. For the low initial condition, only the basal expression is present in the pre-run, while for the high initial condition, the whole system is taken into account. For the pre-run in the extended system (2.58), the promoters are assumed to be inactive ($A_f = A_b = 0$) and the enzyme is taken at the steady state level. Taking the experimental conditions into account, the doxycycline concentrations 0 and $19.5 \mu M$ are applied in the pre-run for the low and high initial conditions, respectively. Afterwards, doxycycline concentrations are

replaced with the actual values and the simulation continues until the concentration of the protein reaches a pre-defined threshold. In order to define this threshold based on experimental assumptions, we get the geometric mean of the steady state concentrations of the protein calculated at the geometric mean of the bistability area. Figures 2.27 and 2.28 show transition rates for different dox concentrations in system (2.58) in the closed-loop setting with and without dimerization. In feedback loops, the expression range, which is the ratio between the basal and the maximal induced gene expression, plays an important role. Therefore, we tune the doxycycline concentration and the expression range independently in the prediction of the transition rates. The transition rates obtained from experimental data and the ones predicted by the stochastic simulation algorithm are compared in the two-dimensional parameter space containing the concentration of doxycycline and the expression range (Figures 2.27–2.29).

Chapter 3

Conclusions

We derived an analytical method that allows us to decompose the total variability of a component into individual contributions of all other components in a network. Noise decomposition helps us determine how much of the variability in a specific component results from a specific kinetic reaction and therefore illustrates the importance of different system modifications by adding or omitting biological processes. In particular, we showed the effect of nonlinear degradation on RNA's variability in gene regulatory networks. We then formulated a general relation between the strength of correlations among different components, and the decomposed normalized noise. Different components of a network can be correlated due to different co-regulation processes. In the presence of multiple co-regulation processes, the individual correlations induced by each process equals the ratio between the extrinsic normalized noise induced by such processes and the total normalized noise of a component.

Noise in bistable networks plays an important role in transitions between steady states. The transitions can be independently modulated by deterministic processes (drift) and random fluctuations (diffusion). The Fokker-Planck equation (FPE) is a suitable tool to calculate the transition rates and can be conveniently used for single variable systems. However, most feedback loop systems are multicomponent systems. In order to involve the variability of all components of a network, we applied FPE to a multidimensional system in an open-loop setting to obtain the total diffusion, and used a quasi-steady state assumption to reduce the system to the slowest variable. The open-loop function can be used to identify the steady-state expression of the output and consequently map accurately the steady-state expression levels for the closed-loop system. With the drift and total diffusion, after reclosing the loop, we calculated the MFPT for the reduced closed-loop system which was in good agreement with the results

of stochastic simulation of the multidimensional system. It is important to note that the accurate approximation of the open-loop system is an important but not sufficient condition for a good prediction of the MFPT. Only the opening at the slowest variable warrants an accurate prediction of MFPT. This is an important difference to classical deterministic loop opening, where it does not matter where to open the loop.

It should be noted that in real systems, fluctuations have short but non-zero correlation time. This short memory results in a hidden nonlinearity in the system and can be shown mathematically by Stratonovich method. When different components of a network interact multiplicatively, the system description with uncorrelated white noises in the Ito-interpretation does not predict correctly the system behavior. This is not surprising because it has been known that in the presence of high-order reactions, the FPE with independent white fluctuations is not accurate [14, 50]. Different approaches have been introduced to resolve the discrepancy [46]. In this work, we included correlations between the two interacting components and used the Stratonovich interpretation. Our approach explained both the noise-induced shift in the open-loop function and the high variance in the output. Furthermore, the predicted MFPTs were shown to be accurate at a broad range of realistic values of external noise.

The above results indicate that the drift and diffusion obtained by the open-loop approach faithfully reflect the stochastic system dynamics and can be used to calculate the MFPT even when the expectation value of the output is shifted by external noise. The loop opening facilitates the calculation of time scales of the reactions and the mean and variance of the output. An appropriate function can be fitted to the measured open-loop mean and variance to obtain the drift and diffusion, which are then used to determine the MFPT.

Published articles related to the thesis:

F. Maleki and A. Becskei.

An open-loop approach to calculate noise-induced transitions.

Under review.

Bibliography

- [1] David Angeli, James E Ferrell, and Eduardo D Sontag. Detection of multi-stability, bifurcations, and hysteresis in a large class of biological positive-feedback systems. *Proceedings of the National Academy of Sciences of the United States of America*, 101(7):1822–1827, 2004. [24](#), [45](#)
- [2] Nils Berglund. Kramers’ law: Validity, derivations and generalisations. *arXiv preprint arXiv:1106.5799*, 2011. [9](#)
- [3] Nils Berglund and Barbara Gentz. The eyring-kramers law for potentials with nonquadratic saddles. *arXiv preprint arXiv:0807.1681*, 2008. [9](#)
- [4] William J Blake, Gábor Balázsi, Michael A Kohanski, Farren J Isaacs, Kevin F Murphy, Yina Kuang, Charles R Cantor, David R Walt, and James J Collins. Phenotypic consequences of promoter-mediated transcriptional noise. *Molecular cell*, 24(6):853–865, 2006. [12](#)
- [5] Nicolas E Buchler and Matthieu Louis. Molecular titration and ultrasensitivity in regulatory networks. *Journal of molecular biology*, 384(5):1106–1119, 2008. [50](#)
- [6] Li Cao and Da-jin Wu. Cross-correlation of multiplicative and additive noises in a single-mode laser white-gain-noise model and correlated noises induced transitions. *Physics Letters A*, 260(1):126–131, 1999. [6](#), [11](#)
- [7] Jyotipratim Ray Chaudhuri, Sudip Chattopadhyay, and Suman Kumar Banik. Multiplicative cross-correlated noise induced escape rate from a metastable state. *The Journal of chemical physics*, 128(15):154513, 2008. [6](#), [12](#), [35](#)
- [8] Zhang Cheng, Feng Liu, Xiao-Peng Zhang, and Wei Wang. Robustness analysis of cellular memory in an autoactivating positive feedback system. *FEBS letters*, 582(27):3776–3782, 2008. [12](#)

- [9] Bärbel Finkenstädt, Dan J Woodcock, Michal Komorowski, Claire V Harper, Julian RE Davis, Mike RH White, David A Rand, et al. Quantifying intrinsic and extrinsic noise in gene transcription using the linear noise approximation: An application to single cell data. *The Annals of Applied Statistics*, 7(4):1960–1982, 2013. [8](#)
- [10] David Frigola, Laura Casanellas, José M Sancho, and Marta Ibañes. Asymmetric stochastic switching driven by intrinsic molecular noise. *PLoS One*, 7(2):e31407, 2012. [6](#), [12](#)
- [11] Andrzej Fuliński and Tomasz Telejko. On the effect of interference of additive and multiplicative noises. *Physics Letters A*, 152(1):11–14, 1991. [12](#)
- [12] Pulak Kumar Ghosh, Bidhan Chandra Bag, and Deb Shankar Ray. Noise correlation-induced splitting of kramers’ escape rate from a metastable state. *The Journal of chemical physics*, 127(4):044510, 2007. [12](#)
- [13] Daniel T Gillespie. Exact stochastic simulation of coupled chemical reactions. *The journal of physical chemistry*, 81(25):2340–2361, 1977. [10](#)
- [14] Ramon Grima, Philipp Thomas, and Arthur V Straube. How accurate are the nonlinear chemical fokker-planck and chemical langevin equations? *The Journal of chemical physics*, 135(8):084103, 2011. [35](#), [58](#)
- [15] John Guckenheimer and Philip Holmes. *Nonlinear oscillations, dynamical systems, and bifurcations of vector fields*, volume 42. Springer Science & Business Media, 2013. [1](#)
- [16] Henryk Gzyl. *Noise-induced transitions: Theory and applications in physics, chemistry and biology*, volume 11. Springer, 1988. [6](#), [11](#)
- [17] Rutger Hermsen, David W Erickson, and Terence Hwa. Speed, sensitivity, and bistability in auto-activating signaling circuits. *PLoS Comput Biol*, 7(11):e1002265, 2011. [12](#)
- [18] Chieh Hsu, Vincent Jaquet, Farzaneh Maleki, and Attila Becskei. Contribution of bistability and noise to cell fate transitions determined by feedback opening. *Journal of Molecular Biology*, 2016. [49](#)
- [19] Tobias Jahnke and Wilhelm Huisinga. Solving the chemical master equation for monomolecular reaction systems analytically. *Journal of mathematical biology*, 54(1):1–26, 2007. [7](#)

- [20] Tobias Jahnke and Wilhelm Huisinga. A dynamical low-rank approach to the chemical master equation. *Bulletin of mathematical biology*, 70(8):2283–2302, 2008. [7](#)
- [21] JAM Janssen. The elimination of fast variables in complex chemical reactions. ii. mesoscopic level (reducible case). *Journal of statistical physics*, 57(1-2):171–185, 1989. [26](#)
- [22] Joanna Jaruszewicz, Pawel J Zuk, and Tomasz Lipniacki. Type of noise defines global attractors in bistable molecular regulatory systems. *Journal of theoretical biology*, 317:140–151, 2013. [12](#)
- [23] Thomas B Kepler and Timothy C Elston. Stochasticity in transcriptional regulation: origins, consequences, and mathematical representations. *Biophysical journal*, 81(6):3116–3136, 2001. [12](#)
- [24] Hendrik Anthony Kramers. Brownian motion in a field of force and the diffusion model of chemical reactions. *Physica*, 7(4):284–304, 1940. [12](#)
- [25] Hiroyuki Kuwahara and Russell Schwartz. Stochastic steady state gain in a gene expression process with mrna degradation control. *Journal of The Royal Society Interface*, page rsif20110757, 2012. [12](#), [16](#)
- [26] Yuri A Kuznetsov. *Elements of applied bifurcation theory*, volume 112. Springer Science & Business Media, 2013. [2](#)
- [27] Ian J Laurenzi. An analytical solution of the stochastic master equation for reversible bimolecular reaction kinetics. *The Journal of Chemical Physics*, 113(8):3315–3322, 2000. [7](#)
- [28] Ioannis Lestas, Johan Paulsson, Nicholas E Ross, and Glenn Vinnicombe. *Automatic Control, IEEE Transactions on*, 53(Special Issue):189–200, 2008. [6](#)
- [29] Quan Liu and Ya Jia. Fluctuations-induced switch in the gene transcriptional regulatory system. *Physical Review E*, 70(4):041907, 2004. [12](#)
- [30] Reinhard Mahnke, Jevgenijs Kaupuzs, and Ihor Lubashevsky. *Physics of stochastic processes: how randomness acts in time*. John Wiley & Sons, 2009. [3](#), [4](#)
- [31] Imre Májer, Amirhossein Hajihosseini, and Attila Becskei. Identification of optimal parameter combinations for the emergence of bistability. *Physical biology*, 12(6):066011, 2015. [24](#)

- [32] Thiago G Mattos, Carlos Mejía-Monasterio, Ralf Metzler, and Gleb Oshanin. First passages in bounded domains: When is the mean first passage time meaningful? *Physical Review E*, 86(3):031143, 2012. [8](#)
- [33] Dongcheng Mei, Guangzhong Xie, Li Cao, and Dajin Wu. Mean first-passage time of a bistable kinetic model driven by cross-correlated noises. *Physical Review E*, 59(4):3880, 1999. [12](#)
- [34] Johan Paulsson. Models of stochastic gene expression. *Physics of life reviews*, 2(2):157–175, 2005. [11](#)
- [35] G.A. Pavliotis. *Stochastic Processes and Applications: Diffusion Processes, the Fokker-Planck and Langevin Equations*. Springer, 2014. [7](#)
- [36] Juan M Pedraza and Alexander van Oudenaarden. Noise propagation in gene networks. *Science*, 307(5717):1965–1969, 2005. [11](#)
- [37] Giuseppe Pesce, Austin McDaniel, Scott Hottovy, Jan Wehr, and Giovanni Volpe. Stratonovich-to-itô transition in noisy systems with multiplicative feedback. *Nature communications*, 4, 2013. [11](#)
- [38] Hong Qian. Cooperativity in cellular biochemical processes: Noise-enhanced sensitivity, fluctuating enzyme, bistability with nonlinear feedback, and other mechanisms for sigmoidal responses. *Annual review of biophysics*, 41:179–204, 2012. [12](#)
- [39] Navneet Rai, Rajat Anand, Krishna Ramkumar, Varun Sreenivasan, Sugat Dabholkar, KV Venkatesh, and Mukund Thattai. Prediction by promoter logic in bacterial quorum sensing. *PLoS Comput Biol*, 8(1):e1002361, 2012. [24](#)
- [40] Hannes Risken. *The Fokker-Planck Equation. Methods of Solution and Applications*, vol. 18 of. 1989. [7](#), [13](#)
- [41] Nitzan Rosenfeld, Michael B Elowitz, and Uri Alon. Negative autoregulation speeds the response times of transcription networks. *Journal of molecular biology*, 323(5):785–793, 2002. [12](#)
- [42] Marc R Roussel and Rui Zhu. Reducing a chemical master equation by invariant manifold methods. *The Journal of chemical physics*, 121(18):8716–8730, 2004. [7](#)
- [43] Álvaro Sánchez and Jané Kondev. Transcriptional control of noise in gene expression. *Proceedings of the National Academy of Sciences*, 105(13):5081–5086, 2008. [11](#), [35](#)

- [44] M Scott. *Applied stochastic processes in science and engineering*. Citeseer, 2011. [7](#), [14](#)
- [45] Matthew Scott, Brian Ingalls, and Mads Kaern. Estimations of intrinsic and extrinsic noise in models of nonlinear genetic networks. *Chaos: An Interdisciplinary Journal of Nonlinear Science*, 16(2):026107, 2006. [11](#), [19](#)
- [46] Vahid Shahrezaei, Julien F Ollivier, and Peter S Swain. Colored extrinsic fluctuations and stochastic gene expression. *Molecular systems biology*, 4(1), 2008. [19](#), [58](#)
- [47] P. S. Swain, M. B. Elowitz, and E. D. Siggia. Intrinsic and extrinsic contributions to stochasticity in gene expression. *Proc. Natl. Acad. Sci.*, 99, 2002. [11](#)
- [48] Mukund Thattai and Alexander Van Oudenaarden. Intrinsic noise in gene regulatory networks. *Proceedings of the National Academy of Sciences*, 98(15):8614–8619, 2001. [11](#)
- [49] Philipp Thomas, Ramon Grima, and Arthur V Straube. Rigorous elimination of fast stochastic variables from the linear noise approximation using projection operators. *Physical Review E*, 86(4):041110, 2012. [26](#)
- [50] Philipp Thomas, Hannes Matuschek, and Ramon Grima. How reliable is the linear noise approximation of gene regulatory networks? *BMC genomics*, 14(Suppl 4):S5, 2013. [35](#), [58](#)
- [51] Abhinav Tiwari and Oleg A Igoshin. Coupling between feedback loops in autoregulatory networks affects bistability range, open-loop gain and switching times. *Physical biology*, 9(5):055003, 2012. [12](#)
- [52] Tsz-Leung To and Narendra Maheshri. Noise can induce bimodality in positive transcriptional feedback loops without bistability. *Science*, 327(5969):1142–1145, 2010. [12](#)
- [53] Nicolaas Godfried Van Kampen. *Stochastic processes in physics and chemistry*, volume 1. Elsevier, 1992. [5](#), [13](#)
- [54] Benjamin Volkmer and Matthias Heinemann. Condition-dependent cell volume and concentration of escherichia coli to facilitate data conversion for systems biology modeling. *PloS one*, 6(7):e23126, 2011. [7](#)
- [55] Stephen Wiggins. *Introduction to applied nonlinear dynamical systems and chaos*, volume 2. Springer Science & Business Media, 2003. [2](#)

Farzaneh Maleki

EMAIL: farzanmaleki83@gmail.com

PHONE: +41 77 4647743

Education

JUN 2012	Ph.D. in Systems Biology
AUG 2016	Biozentrum, University of Basel, Basel, Switzerland
SEP 2007	M.Sc. in Applied Mathematics
SEP 2009	School of Mathematics, Statistics and Computer Science University of Tehran, Tehran, Iran
SEP 2002	B.Sc. in Pure Mathematics
AUG 2006	Department of Mathematics, University of Malayer, Malayer, Iran

Professional Experience

JUN 2012	Research Assistant
AUG 2016	Biozentrum, University of Basel, Basel, Switzerland
JAN 2008	Researcher
JUN 2012	Center of Excellence in Biomathematics University of Tehran, Tehran, Iran
JUN 2010	Research Collaborator
JUN 2012	School of Mathematics Institute for Research in Fundamental Sciences (IPM), Tehran, Iran
JUN 2008	Research Collaborator
SEP 2009	School of Pharmacy Tehran University of Medical Sciences (TUMS), Tehran, Iran

Publications

1. **F. Maleki**, A. Becskei. *An open-loop approach to calculate noise-induced transitions*. Preprint.
2. C. Hsu, V. Jaquet, **F. Maleki**, A. Becskei. *Contribution of bistability and noise to cell fate transitions determined by feedback opening*. *Journal of Molecular Biology* (2016).
3. G. R. Rokni Lamooki, **F. Maleki**, A. Hajihosseini. *A mathematical model for the ICU admission process*. *Communications in Nonlinear Science and Numerical Simulation* **19** (2014) 8-18.
4. A. Hajihosseini, **F. Maleki**, G. R. Rokni Lamooki. *Bifurcation analysis on a generalized recurrent neural network with two interconnected three-neuron components*. *Chaos, Solitons & Fractals* **44** (2011) 1004-1019.
5. **F. Maleki**, B. Beheshti, A. Hajihosseini, G. R. Rokni Lamooki. *The Bogdanov-Takens bifurcation analysis on a three dimensional recurrent neural network*. *Neurocomputing* **73** (2010) 3066-3078.
6. A. Hajihosseini, G. R. Rokni Lamooki, B. Beheshti, **F. Maleki**. *The Hopf bifurcation analysis on a time-delayed recurrent neural network in the frequency domain*. *Neurocomputing* **73** (2010) 991-1005.